THE JOURNAL OF BIOLOGICAL CHEMISTRY
Vol. 278, No. 36, Issue of September 5, pp. 33654–33671, 2003
Printed in U.S.A.

A 16-Residue Peptide Fragment of Macrophage Migration Inhibitory Factor, MIF-(50–65), Exhibits Redox Activity and Has MIF-like Biological Functions*

Received for publication, February 19, 2003, and in revised form, June 6, 2003
Published, JBC Papers in Press, June 9, 2003, DOI 10.1074/jbc.M301735200

Mai Tuyet Nguyen‡, Jürgen Beck§, Hongqi Lue¶, Helge Fünfzig¶, Robert Kleemann‖, Pieter Koolwijk‖, Aphrodite Kapurniotu§‡‡§§, and Jürgen Bernhagen¶ ¶¶**

From the ¶Division of Biochemistry and Molecular Cell Biology, Institute of Biochemistry, University Hospital RWTH Aachen, D-52074 Aachen, ‡‡Laboratory of Bioorganic and Medicinal Chemistry, Institute of Biochemistry, University Hospital RWTH Aachen, D-52074 Aachen, ‡Laboratory of Biochemistry, Institute for Interfacial Engineering, University of Stuttgart, D-70569 Stuttgart, §Physiological-Chemical Institute, University of Tübingen, D-72076 Tübingen, Germany, and ‖The Gaubius Laboratory, Toegepast Natuurwetenschappelijk Onderzoek-Prevention and Health, 2301 Leiden, The Netherlands

Macrophage migration inhibitory factor (MIF) is a cytokine that participates in the host inflammatory response. A Cys-Xaa-Xaa-Cys (C*XX*C)-based thiol-protein oxidoreductase activity of MIF is associated with certain biological functions. Peptides spanning the C*XX*C region of thiol-protein oxidoreductases retain some biochemical properties of the full-length protein. We report on the characterization of C*XX*C-spanning MIF-(50–65) and its serine variant, C57S/C60S-MIF-(50–65). Following disulfide-mediated cyclization, MIF-(50–65) adapted a β-turn conformation comparable with that of β-turn-containing cyclo-57,60-[Asp^{57},Dap^{60}]MIF-(50–65). MIF-(50–65) had a redox potential E'_0 of −0.258 V and formed mixed disulfides with glutathione and cysteine. MIF-(50–65) but not C57S/C60S-MIF-(50–65) had oxidoreductase activity *in vitro*. Intriguingly, MIF-(50–65) exhibited MIF-like cellular activities. The peptide but not its variant had glucocorticoid overriding and proliferation-enhancing activity and stimulated ERK1/2 phosphorylation. MIF-(50–65) and its variant bound to the MIF-binding protein JAB1 and enhanced cellular levels of p27^{Kip1}. As the peptide and its variant were endocytosed at similar efficiency, sequence 50–65 appears sufficient for the JAB1-related effects of MIF, whereas other activities require C*XX*C. Cyclo-57,60-[Asp^{57},Dap^{60}]MIF-(50–65) activated ERK1/2, indicating that C*XX*C-dependent disulfide and β-turn formation is associated with an activity-inducing conformation. We conclude that C*XX*C and sequence 50–65 are critical for the activities of MIF. MIF-(50–65) is a surprisingly short sequence with MIF-like functions that could be an excellent molecular template for MIF therapeutics.

Macrophage migration inhibitory factor (MIF)[1] was discovered 40 years ago as a lymphocyte mediator that inhibited the random migration of macrophages (1). Later on, MIF was rediscovered as a pituitary factor with hormone-like properties (2, 3). Today, MIF is known as a widely expressed pleiotropic cytokine exhibiting a broad range of immune and inflammatory activities, including induction of inflammatory cytokines, nitric oxide and superoxide anion, and regulation of macrophage and lymphocyte proliferation. The immuno-regulatory activities of MIF are based upon transcriptional regulation of inflammatory gene products, modulation of cell proliferation and cell cycle inhibition of p53-mediated apoptosis, and on a number of metabolic effects (summarized in Refs. 4–6). MIF plays a pivotal role in the pathogenesis of a number of immune and inflammatory conditions such as septic shock, rheumatoid arthritis, cancer, and lung diseases. Consequently, MIF-based therapeutic approaches have become of major interest (2, 7–12).

The molecular mechanisms of MIF action have not yet been elucidated. In particular, a membrane receptor for MIF has not been identified. MIF modulates the phosphorylation and activ-

* This work was supported in part Grants Be 1977/1-3 and SFB 542/TP-A7 from the Deutsche Forschungsgemeinschaft (to J. B.) and by a stipend from the Landesgraduiertenförderung Baden-Württemberg (to M. T. N.). The costs of publication of this article were defrayed in part by the payment of page charges. This article must therefore be hereby marked "*advertisement*" in accordance with 18 U.S.C. Section 1734 solely to indicate this fact.

** Recipient of NWO Grant 016.036.061 from the Netherlands Organization for Scientific Research.

§§ To whom correspondence may be addressed: Laboratory of Bioorganic and Medicinal Chemistry, Institute of Biochemistry, University Hospital RWTH Aachen, Germany. Tel.: 49-241-8088844; Fax: 49-241-8082427; E-mail: akapurniotu@ukaachen.de.

¶¶ To whom correspondence may be addressed: Division of Biochemistry and Molecular Cell Biology, Institute of Biochemistry, University Hospital RWTH Aachen, Pauwelsstrasse 30, D-52074 Aachen, Germany. Tel.: 49-241-8088840; Fax: 49-241-8082427; E-mail: jbernhagen@ukaachen.de.

[1] The abbreviations used are: MIF, macrophage migration inhibitory factor; MIF-(50–65), sequence region 50–65 of human MIF; biotin-MIF-(50–65), analog of MIF-(50–65) with N-terminally linked biotinamidocaproate moiety; biotin-C57S/C60S-MIF-(50–65), analog of C57S/C60S-MIF-(50–65) with N-terminally linked biotinamidocaproate moiety; C57S/C60S-MIF-(50–65) or Ser-MIF-(50–65), bis-serine variant of MIF-(50–65) with Cys → Ser changes at positions 57 and 60; C60SMIF, MIF mutant with a Cys → Ser mutation at residue 60; CALC, Cys-Ala-Leu-Cys motif; C*XX*C, Cys-Xaa-Xaa-Cys motif; CSN5, COP9 signalosome subunit 5; cyclo-MIF-(50–65), cyclo-^{57,60}-[Asp^{57},Dap^{60}]MIF-(50–65); DTT, dithiothreitol; Fluo-MIF-(50–65), analog of MIF-(50–65) with N-terminally linked carboxyfluorescein moiety; Fluo-C57S/C60S-MIF-(50–65), analog of C57S/C60S-MIF-(50–65) with N-terminally linked carboxyfluorescein moiety; Grx, glutaredoxin; HED, bis-(2-hydroxyethyl)-disulfide; JAB1, c-Jun activation domain binding protein 1; LPS, lipopolysaccharide; PDI, protein-disulfide isomerase; rMIF, biologically active recombinant wild-type human MIF; TPOR, thiol-protein oxidoreductase; Trr, thioredoxin reductase; Trx, thioredoxin; HPLC, high pressure liquid chromatography; RP-HPLC, reverse phase HPLC; MPAK, mitogen-activated protein kinase; MALDI-TOF-MS, matrix-assisted laser desorption ionization/time-of-flight-mass spectrometry; Fmoc, 9-fluorenylmethoxycarbonyl; FCS, fetal calf serum; PBS, phosphate-buffered saline; ERK, extracellular signal-regulated kinase; VEGF, vascular endothelial cell growth factor; bFGF, basic fibroblast growth factor; DMEM, Dulbecco's modified Eagle's medium; DTT, dithiothreitol; MHC, major histocompatibility complex; CFSE, 5(6)-carboxyfluorescein-*N*-hydroxysuccinimide ester; SPPS, solid phase synthetic protocols; DEX, dexamethasone; TNF, tumor necrosis factor; hMVEC, human microvascular endothelial cells; GCOR, glucocorticoid overriding; GIF, glycosylation-inhibiting factor; Dap, diaminopropionic acid.

ity of protein kinases (13) and interacts with and regulates the activity of the transcriptional co-activator JAB1/CSN5 (14, 15). However, it is currently unclear what the upstream molecular events of these effects are. It has been considered that an observed catalytic thiol-protein oxidoreductase (TPOR) activity of MIF could be responsible, at least in part, for the cellular functions of MIF.

The TPOR family of proteins encompasses enzymes such as thioredoxin (Trx), glutaredoxin (Grx), protein-disulfide isomerase (PDI), or the disulfide bond proteins, with Trx being the prototype member of the family. TPORs catalyze the reduction of protein disulfides in a cysteine-based dithiol/disulfide-dependent process, and some family members also serve as potent protein folding catalysts. TPOR proteins share a common Cys-Xaa-Xaa-Cys (C*XX*C) consensus motif within a homologous so-called Trx-fold, where the C*XX*C motif is located at the N terminus of an α-helix. MIF contains a C*XX*C TPOR consensus motif, with the residues Ala and Leu placed between the cysteines and also contains additional conserved residues that are frequently found N-terminally of the C*XX*C region (16). Although the overall three-dimensional structure of the MIF monomer shows a remote resemblance to the Trx monomer, MIF is not structurally homologous to the TPOR proteins, and the Cys-Ala-Leu-Cys (CALC) redox motif of MIF lies at the N terminus of a β-strand element with Cys^{57} located in the preceding loop (17, 18) rather than in a Trx-like fold. MIF exhibits TPOR activity *in vitro* being able to catalyze the reduction of both insulin and small molecular weight compound disulfides (19–21). Mutation of the C*XX*C cysteines of MIF results in partly or fully immunologically inactive MIF protein, an observation that has led to the suggestion that the TPOR activity of MIF is responsible in part for its immunological and cellular activities (14, 19–23). In addition, an involvement of MIF in the regulation of cellular redox processes is likely, as in addition to the above-mentioned findings, MIF was found to bind to and regulate the peroxiredoxin (24) and to inhibit oxidative stress-induced apoptosis (25). It has been speculated that the enzymatic activity of MIF could serve to bypass a potential receptor-mediated signaling pathway, to assist in MHC II antigen processing, or to mediate additional intracellular activities of MIF (6, 21, 26).

Thus, although MIF is not structurally related to the TPOR proteins, it shares with these proteins catalytic TPOR activity *in vitro* and the capability to participate in redox regulation *in vivo*. Moreover, MIF shares additional intriguing properties with Trx. Trx or adult T cell leukemia-derived factor plays a role in the regulation of cellular redox stress (27, 28) through its TPOR activity. Also, Trx, although originally discovered as a TPOR and ribonucleotide reductase enzyme, has recently been re-defined as a cytokine and immune mediator (29, 30).

The redox potential of the TPOR proteins is governed by both the overall three-dimensional structural constraints of the respective enzymes and the sequence composition of the C*XX*C motif together with the surrounding residues of the Trx fold (31–35). Short peptide fragments derived from TPORs that span the C*XX*C region and artificial mimetics thereof have therefore been investigated to correlate the sequence requirements with the redox potentials of the corresponding enzymes and to assess the influence of three-dimensional structural constraints (34–37). Of note, some of these small peptides were recently shown to function as catalysts of protein folding processes (35).

As the three-dimensional structure of the C*XX*C region of MIF only has minor similarities to the C*XX*C/Trx-fold structure of the TPORs but MIF nevertheless exhibits TPOR-like activity, we surmised that during catalysis, the structure of MIF may be partially unfolded or changed. In this respect, it is noteworthy of mentioning that it has been suggested that a mono- or dimeric structure, possibly with slightly different conformational properties, but not the MIF trimer, may be the predominant MIF species under physiological conditions (38). Interestingly, thioredoxin reductase (Trr), a member of the TPOR family, also does not contain an apparent Trx fold structure but otherwise shares similar redox properties with the TPOR proteins, indicating that it may undergo a marked conformational change during catalysis (39). Computer-based secondary structure predictions had shown previously (19) that the C*XX*C sequence region of MIF has a high β-turn-forming propensity that is comparable with that of the TPOR enzymes. If altered conformational elements were involved in MIF-mediated redox catalysis and biological activity, it thus appeared possible that MIF-derived peptides featuring such properties could function as MIF mimetics.

Here we elected a 16-residue MIF peptide fragment spanning the CALC motif of MIF and encompassing the residues that are part of the predicted β-turn. The peptide ranged from residue Phe-50 to Ile-65 and was termed MIF-(50–65). It contained additional turn-stabilizing residues flanking the C*XX*C motif and covered the aromatic residue (Phe-50) which is part of extended C*XX*C sequence patterns according to Ellis *et al.* (16).

The peptide and its C57S/C60S bis-serine, biotinylated, and fluorescein-modified variants as well as a peptide analog covalently cyclized by a lactam bridge were synthesized by solid phase Fmoc chemistry, HPLC-purified, and investigated for their conformational, redox, and *in vitro* TPOR catalytic properties. Applying a variety of immunological and cellular assays that are characteristic of the immunological, inflammatory, and cellular functions of MIF *in vivo*, we then asked whether the 16-meric peptide may have retained MIF-like functional properties and could serve to mimic cellular MIF activities.

MATERIALS AND METHODS

Chemicals, Buffers, Recombinant MIF, and General Cell Culture Reagents—Protected amino acids were purchased from Rapp Polymer (Tübingen, Germany). All other peptide synthesis reagents were obtained from Bachem (Heidelberg, Germany). 5(6)-Carboxyfluorescein-*N*-hydroxysuccinimide ester (CFSE) was from Roche Diagnostics. Analytical grade acetonitrile was from Mallinckrodt Chemical Works and from Merck. Trifluoroacetic acid, reduced and oxidized glutathione (GSH and GSSG), L-cysteine and L-cystine, 1,4-dithiothreitol (DTT), insulin, bis-(2-hydroxyethyl)-disulfide (HED), β-nicotinamide adenine dinucleotide phosphate (reduced form, NADPH), glutathione reductase, L-3,4-dihydroxyphenylalanine methyl ester, sodium peroxidate, lipopolysaccharide O111:B4 (LPS), and dexamethasone (DEX) were obtained from Sigma. All general cell culture reagents such as media, supplements, antibiotics, and serum (for the latter, see below) were from Invitrogen. NIH 3T3 and THP-1 cells were bought from the German Society for Microorganisms and Cell Cultures (DSMZ, Braunschweig, Germany). Cells were cultured by routine protocols at 37 °C in a humidified incubator with 5% CO_2. Streptavidin-conjugated magnetic beads (Dynabeads M-280 streptavidin) were bought from Dynal Biotec ASA (Oslo, Norway). Streptavidin-coupled nanoparticles were a kind gift from Dr. G. Tovar (Fraunhofer IGB, Stuttgart, Germany). Biologically active recombinant human MIF (rMIF) was expressed, purified, and refolded as described previously (40). Vascular endothelial cell growth factor (VEGF) was purchased from REALITech (Braunschweig, Germany), and basic fibroblast growth factor (bFGF) was bought from PeproTech (Rocky Hill, NJ). Crude endothelial cell growth factor was prepared from bovine hypothalamus as described by Maciag *et al.* (41). [^{3}H]Thymidine was from Amersham Biosciences. Anti-phospho-ERK1/2 (E4, sc-7383) and anti-ERK1/2 (C16, sc-93) antibodies were obtained from Santa Cruz Biotechnology (Heidelberg, Germany). Miscellaneous chemicals, solvents, and salts were from Sigma. All reagents were of the highest grade commercially available.

Synthesis and Purification of the MIF-derived Peptides MIF-(50–65) and C57S/C60S-MIF-(50–65) and Their Biotinylated, Fluoresceinated, Lactam-bridged Derivatives, and Control Peptides—Peptide synthesis

was performed by solid phase synthetic protocols (SPPS) as described by us previously (42). The N terminus of the peptides was acetylated and the C terminus amidated. For synthesis of C57S/C60S-MIF-(50–65), serine residues were coupled at positions 57 and 60 instead of the active site cysteines. Biotinylation of MIF-(50–65) and C57S/C60S-MIF-(50–65) was performed at the N terminus of the fully protected and resin-bound peptides using normal coupling protocols in a mixture (2/1) of dimethylformamide and *N*-methyl-2-pyrrolidone, and an aminocaproate residue was also incorporated as a spacer between biotin and the peptide. N-terminal fluorescein-labeled forms of MIF-(50–65) and C57S/C60S-MIF-(50–65) were obtained by reaction of the side chain-protected, resin-bound peptides with CFSE which was applied in 1.7–2.3 molar excess. Reactions with CFSE were carried out for 3 h in a mixture (3/1) of dimethylformamide and dimethyl sulfoxide (Me_2SO). Synthesis and side chain-to-side chain cyclization of cyclo^{57,60}-[Asp^{57},Dap^{60}]MIF-(50–65) and the linear control peptide [Asp^{57},Dap^{60}]MIF-(50–65) was performed according to a procedure published previously (42).

Briefly, as to the SPPS procedure in general, synthesis was performed on Rink resin applying the 9-fluorenylmethoxycarbonyl (Fmoc) group for temporary protection of the α-amino function. Side chains of trifunctional amino acids were protected with *t*-butyl (Ser), trityl (Cys), Trt (His), and *t*-butyl (Glu). Deprotection with simultaneous cleavage of the peptide from the resin was performed by treatment with 95% trifluoroacetic acid, 2.5% ethanedithiol, 2.5% water. Following evaporation of trifluoroacetic acid under vacuum at 30 °C, 10% acetic acid was added to the resulting product, and the aqueous phase was extracted three times with diethyl ether. The aqueous phase was then lyophilized. The obtained crude product, which was obtained in its reduced form and in a purity of about 90%, was further purified by C18 reverse phase (RP) HPLC (250 × 8 mm; 100 Å pore size, 7 μm particle size; Grom, Herrenberg, Germany). Elution of the peptides was achieved with two different water/acetonitrile elution programs. The first program consisted of a gradient of 10% B to 90% B between 1 and 31 min; and the second elution program was 0–7 min at 30% B, followed by a gradient from 30 to 60% B for 30 min, with buffer A 0.058% trifluoroacetic acid; buffer B 90% acetonitrile, 0.05% trifluoroacetic acid; flow rate 2 ml/min, and peptides were detected at 214 nm. The identity and purity of the peptides was verified by mass spectrometric analysis (see below and figure legends for details) and analytical HPLC. Following lyophilization, purified reduced peptide was stored at −20 °C until used further. Disulfide bridge-containing forms of the peptides were obtained by air oxidation in 0.1 M ammonium bicarbonate at a peptide concentration of 0.1 mg/ml. The oxidized peptide as well as the mixed disulfide species were collected on dry ice, deep frozen, and lyophilized. After lyophilization, the sample was dissolved in 10% acetic acid and immediately purified by HPLC (see above). For preparation of the purified reduced peptide see below. Mutant peptide C57S/C60S-MIF-(50–65) and the biotinylated, fluoresceinated, and side chain-to-side chain cyclized peptides were purified directly from their corresponding crude synthesis products by HPLC. The biotinylated and fluorescein-labeled wild-type derivatives were applied in the biological assays in their reduced forms.

Peptide Verification by Mass Spectrometry, Electrophoresis, and Amino Acid Analysis—The mass spectrometric measurements for peptide verification and determination of the degree of oxidation/reduction and mixed disulfide formation were performed by matrix-assisted laser desorption ionization-time of flight-mass spectrometry (MALDI-TOF-MS; instruments from Shimadzu Kratos Kompact MALDI 3 version 3.0.2, Duisburg, Germany) and G2025A LD-TOF-System Mass Spectrometer from Hewlett-Packard (Böblingen, Germany), and for some preparations by liquid chromatography-coupled electrospray MS (LC-ESMS) on a quadrupole ion trap MS (LCQ from Thermo-Finnigan, San Jose, CA) equipped with an electrospray ion source. Some analyses were performed with an Applied Biosystems API 3000 liquid chromatography-MS. For characterization of some of the side products of the syntheses, fast atom bombardment-MS (VARIAN-MAT 711, Thermo-Finnigan, Bremen, Germany) was applied.

In addition, peptide verification and quantification of the fluoresceinated peptide analogs was performed by 4–12% NuPAGE and silver staining analysis (25) and (quantitative) amino acid analysis on Biotronik amino acid analyzer LC 5001 equipped with fluorescence detection of *o*-phthalaldehyde (Eppendorf, Hamburg, Germany) as described previously (43).

Circular Dichroism Spectrometric Measurements—Near- and far-ultraviolet (UV) circular dichroism (CD) spectropolarimetry was performed essentially as described previously (19). HPLC-purified oxidized and reduced MIF-(50–65), mutant peptide C57S/C60S-MIF-(50–65), and the cyclized lactam-bridged analog were prepared by HPLC as described above and below. For CD analysis, peptides were dissolved in 10 mM Tris-HCl buffer (pH 8.0) at a concentration of 1 mM, briefly sonicated, and diluted from their stock solutions with water to a final concentration of 100 μM. Spectra were recorded within 30 min. For some of the kinetics experiments, reduction of oxidized MIF-(50–65) was followed by incubating the working solution of MIF-(50–65) with 1 mM DTT for a period ranging between 10 min and 6 days. CD spectra are presented as a plot of the mean molar ellipticity per residue ([θ], degrees·cm^2 dmol^{-1}) *versus* the wavelength and represent net spectra, with the spectra of the control buffer solution that was measured in the same cuvette subtracted.

Reduction of the Peptides and Kinetic and Equilibrium Studies—For establishing the HPLC conditions to separate oxidized and reduced MIF-(50–65), purified reduced MIF-(50–65) was generated by reduction of purified oxidized MIF-(50–65) with DTT. Twenty μg of the peptide was dissolved in 20 mM sodium phosphate buffer (pH 7.2) (NaPP), and incubated for 3 h at 30 °C in a 100-μl reaction volume in the presence of 10 mM DTT. Afterward, 40 μl of 1 M H_3PO_4 was added to quench the reaction by reducing the pH to 2. The sample was immediately loaded on an analytical C18 RP-HPLC column (125 × 4 mm; 100-Å pore size, 5-μm particle size; Grom, Herrenberg, Germany). Elution was performed with a linear acetonitrile/water gradient (first gradient) as described above at a flow rate of 1 ml/min. Absorbance was monitored at 220 nm.

For the equilibrium and redox potential studies, the reactions were initiated by mixing equal volumes of 20 μg of MIF peptide fragment 50–65 and small molecular weight reductant. The final reaction volume was 100 μl. Oxidized MIF-(50–65) was generally equilibrated with a reference redox buffer containing varying ratios of GSH/GSSG or cysteine/cystine at a total concentration of 50 mM of redox cofactor. This corresponded to a large excess of the reference redox molecules over the peptide concentration (~400–500-fold for the reduced cofactor and 10–80-fold for the oxidized reference). Incubations were performed at 30 °C in 100 mM sodium phosphate buffer (pH 7.0) containing 1 mM EDTA for the indicated time intervals. Only in the preliminary scouting experiments, concentrations of the oxidized redox reference were in the concentration range of the peptide in some occasions. However, these experiments were not used for the quantification of the redox potential of MIF-(50–65). Reactions were stopped by adding 40 μl of 1 M H_3PO_4 to the 100 μl of the reaction mixture.

Glutathione ratios in the preliminary experiments were 50/10, 50/1, and 50/0.001. For the equilibrium studies and redox potential determinations with glutathione and cysteine, GSH/GSSG, and cysteine/cystine ratios of 42/8, 43/7, 44/6, 45/5, 46/4, 47/3, and 48/2 were applied. The kinetic studies were performed at a ratio of 42/8 for both GSH/GSSG and cysteine/cystine.

Following quenching with phosphoric acid, the samples were separated by C18 HPLC as above, and the peak areas of the reduced, oxidized, and mixed disulfide species of the peptide were quantitated. In some experiments, peaks were collected and subjected to MALDI-TOF-MS (see above) to identify the oxidation state or mixed disulfide species.

For calculating the redox potential of MIF-(50–65), the equilibrium constant K_{ox} was determined according to the following Equation 1,

$$K_{ox} = \frac{[P_{ox}]\,[GSH]^2}{[P_{red}]\,[GSSG]} \qquad K_{ox} = \frac{[P_{ox}]\,[Cys]^2}{[P_{red}]\,[cystine]} \qquad \text{(Eq. 1)}$$

with $[P_{ox}]$ and $[P_{red}]$ representing the fraction of oxidized and reduced MIF-(50–65), respectively, as determined by the corresponding HPLC peak areas following the equilibrium incubations. [GSH] and [GSSG] and [Cys] and [cystine] represent the concentrations of the reduced and oxidized redox cofactors applied. The determination of K_{ox} through this equation is based on the assumption that each step in the multiple equilibria that occur in thiol/disulfide exchange reactions may be treated as a two-state model (principle of detailed balancing (36, 44)). Thus, K_{ox} could be calculated although only one of the mono-mixed disulfide species could be identified and quantitated by HPLC in this study. K_{ox} values were calculated for both the glutathione and cysteine reference using all seven ratios applied. K_{ox} was calculated by two ways as follows: (*a*) the seven K_{ox} values were applied to calculate "K_{ox} mean," and (*b*) the above equation was transformed into a linear regression type of equation $y = m \times x$ and K_{ox} determined from the m value. For both ways, K_{ox} was then used to calculate the redox potential E'_0 according to the Nernst Equation 2:

$$E'_0 = E'_0(\text{R-SH/R-SS-R}) - 0.03 \log K_{ox} \qquad \text{(Eq. 2)}$$

with E'_0(R-SH/R-SS-R) representing the standard redox potential for GSH/GSSG or cysteine/cystine. Values of −0.205 and −0.223 V were assumed according to Szajewski and Whitesides (45) and Millis *et al.* (46), respectively.

The validity of the approach of assuming a two-state model was confirmed by the fact that the obtained values for K_{ox}/E'_0 were nearly identical for the glutathione and cysteine redox references, because, when using the cysteine/cystine pair, no significant fractions representing mixed disulfides were obtained (see "Results").

Enzymatic Assays—The catalytic activity of MIF-(50–65) was evaluated by two different enzymatic assays. The redox activity was addressed using the insulin reduction assay following a protocol described previously (19, 47). MIF-(50–65) was added to the assay from a 1 mM stock solution in 20 mM NaPP and tested at a final concentration of 40 μM.

Tautomerase activity was measured using the D-dopachrome tautomerase test as described previously (48). Briefly, a fresh solution of D-dopachrome methyl ester was prepared by mixing 4 mM L-3,4-dihydroxyphenylalanine methyl ester with 8 mM sodium peroxidate for 5 min at room temperature and then placed directly on ice before use. Activity was then determined at room temperature by adding 100 μl of dopachrome methyl ester to a cuvette containing 800 μl of 25 mM potassium phosphate buffer (pH 6.0) and 0.5 mM EDTA. After 30 s, 100 nM MIF or 3.3 μM MIF peptide was added to the cuvette, and the resulting decrease in absorbance at 475 nm was followed for 4 min using a Speckol spectrophotometer (Jena Analytics, Jena, Germany).

Glucocorticoid Overriding Assay—Glucocorticoid counter-regulating activity of MIF, MIF-(50–65), and its bis-serine variant was assayed using a modification of the glucocorticoid overriding test described previously (3). Briefly, overriding by MIF and the peptides of the anti-inflammatory effect of DEX was analyzed through measuring LPS-stimulated tumor necrosis factor (TNF) production by THP-1 cells. Cells were taken from an early passage and were used no later than 3 weeks following thawing a freeze-down stock. Shortly before the assay, THP-1 cells were plated at a concentration of 1×10^6 cells/ml and were incubated for 1 h with 10^{-9} M DEX and rMIF or the peptides. MIF was used at concentrations ranging from 0.016 to 160 nM. The best overriding effect was observed with a concentration of 0.16 nM. This concentration was then used for comparison with the effects of the peptides. The peptides were tested at 50 nM, 1 μM, and 3.3 μM. Peptide concentrations at 50 nM and 1 μM did not show any measurable overriding activity (data not shown). LPS was added at a concentration of 1 μg/ml together with another aliquot of rMIF or the peptides, and cells were incubated further for 4 h. Culture supernatants were prepared and analyzed for TNF content using a commercial TNF enzyme-linked immunosorbent assay (R&D Systems GmbH, Wiesbaden, Germany).

Endothelial Cell Proliferation Assay—Human foreskin microvascular endothelial cells (hMVEC) were isolated and characterized as described previously (49, 50). Isolated cells were cultured on gelatin-coated dishes in M199 medium supplemented with 20 mM HEPES buffer (pH 7.3), containing 10% human serum, 10% FCS, 150 μg/ml endothelial cell growth factor, 2 mM glutamine, 5 units/ml heparin, as well as 100 IU/ml penicillin and 100 μg/ml streptomycin (pen/strep).

Proliferation of endothelial cells was determined by the incorporation of [^{3}H]thymidine into DNA as reported previously (51). Briefly, confluent cultures of endothelial cells were detached by trypsin/EDTA solution, allowed to adhere, and spread at a density of 10^4 cells per cm^2 on gelatin-coated dishes in M199/HEPES medium supplemented with 10% FCS and pen/strep. After 18 h, the cells were incubated with VEGF at a concentration of 6.25 ng/ml, bFGF (6.25 ng/ml), or PBS (control) in M199/HEPES medium containing pen/strep and 10% FCS and were incubated with rMIF at the indicated concentrations, with the MIF-derived peptides at concentrations of 50 nM, 330 nM, 1 μM, and 3.3 μM, or with control buffer (NaPP). The added volume of the control buffer always corresponded to that of the highest peptide concentration. After 48 h, a tracer amount of [^{3}H]thymidine (0.25 μCi per 1.1 cm^2 well) was added, and the cells were incubated for 6 h. Subsequently, the cells were washed with PBS, and ^{3}H-labeled DNA was fixed with methanol, precipitated in 5% trichloroacetic acid, dissolved in 0.5 ml of 0.3 M sodium hydroxide, and counted in a liquid plate scintillation counter.

Induction of Phosphorylated ERK1/2—1×10^6 NIH 3T3 fibroblasts (passage 10–15) were plated in a 10-cm cell culture plate and incubated in DMEM containing 10% FCS for 24 h. Medium was changed and cells cultured in DMEM containing 0.5% FCS for 24–48 h. Lyophilized MIF-(50–65), bis-serine MIF-(50–65), biotin-MIF-(50–65), biotin-bis-serine-MIF-(50–65), and cyclo-MIF-(50–65) were reconstituted in NaPP buffer at a concentration of 530 μM, and peptide solutions were added to the cells at a final concentration of 50 nM, 300 nM, 1 μM, and 3.3 μM. Controls were incubated with NaPP alone (volume according to the highest peptide concentration). Some plates were treated with 8 nM rMIF. Incubations were stopped at the indicated times (0–30 min) by washing the cells twice with cold PBS. Cells were then lysed with RIPA buffer (PBS (pH 7.4) containing 1% Igepal CA-630, 0.5% sodium deoxycholate, 0.1% SDS, 1 mM EDTA, 1× proteinase inhibitor mixture I (Roche Diagnostics, Mannheim, Germany), and 1 mM sodium orthovanadate) and cellular proteins fractionated in 13.5% SDS-PAGE or 4–12% NuPAGE gels. Following transfer to nitrocellulose filter, Western blots were performed essentially as described previously (14), probed with anti-phospho-ERK1/2 antibody, and developed with the Super Signal West Dura Extended Duration ECL reagent (Pierce/KMF Laborchemie, St. Augustin, Germany). For counterstaining for ERK1/2, the membranes were stripped with 0.5% Tween 20 in TBS (20 mM Tris-HCl (pH 8), 150 mM NaCl) for 30 min and then reprobed with anti-ERK antibody.

Biotin-MIF-(50–65)-JAB1 Pull-down Assay—Pull-down experiments were performed essentially as described previously (14) except that bacterial lysates were used for the *in vitro* transcription/translation reactions. Briefly, ^{35}S-labeled JAB1 protein was generated using bacterial lysates (RINA GmbH, Berlin, Germany). Biotin-MIF-(50–65) or the biotinylated bis-serine variant were added to the lysates, mixtures incubated in low stringency buffer, and complexes precipitated with streptavidin-conjugated magnetic beads (streptavidin Dynabeads, Dynal Inc., Oslo, Norway). Beads were washed and boiled in Laemmli sample buffer and proteins run in a 13.5% SDS-PAGE gel. Detection of bound radiolabeled JAB1 was achieved by drying the gels, incubating them with Amplify™ (Amersham Biosciences) for 30 min, and exposing to a fluorographic film.

Measuring the Effect of MIF and the Peptides on the Levels of $p27^{Kip1}$—To determine the effect of MIF and the peptides on the level of p27^{Kip1}, NIH 3T3 fibroblasts were serum-starved and synchronized as described before (14). Briefly, 0.25×10^6 NIH 3T3 cells were plated in 6-cm tissue culture plates in DMEM supplemented with 10% FCS and antibiotics (100 units/ml pen/strep) and 2 mM L-glutamine. After 6 h, the cells were washed with PBS and incubated overnight in DMEM supplemented with 1% FCS, antibiotics, and L-glutamine. Then the cells were treated with different concentrations of rMIF or the peptides for 24 h at a density of 0.25×10^6 cells per 6-cm culture plate. During this period, the cells remained in the proliferating phase. The cells were harvested, and lysis was performed in RIPA buffer and collected by centrifugation. The supernatants were mixed with 2× Laemmli buffer, boiled, and applied to SDS-PAGE (13.5%) and blotted to a nitrocellulose membrane as described previously (14). Gels and Western blots on the concentration dependences were performed with the NuPAGE (4–12%) system as described (25). Equal loading was adjusted for following Bradford protein assay of the cell lysates (52). A mouse anti-p27 monoclonal IgG (F-8, dilution 1:1000; Santa Cruz Biotechnology or anti-p27 monoclonal antibody, Transduction Laboratories, Lexington, KY) in combination with an anti-mouse peroxidase-coupled antibody was used to detect p27^{Kip1}. Bands were visualized using ECL reagent as above.

Endocytosis Studies of the Peptides—0.2×10^6 NIH 3T3 cells in DMEM supplemented with 10% FCS and antibiotics (100 units/ml pen/strep) and 2 mM L-glutamine were plated on poly-L-lysine-coated coverslips in 3.5-cm tissue culture plates and cultured overnight. Cells were washed 1× with PBS and DMEM with 0.5% FCS was added. The fluorescently labeled peptides were added at a concentration of 10 μM and incubated with the cells for 60 min. Afterward, cells were washed twice with acid glycine buffer (150 mM NaCl, 50 mM glycine (pH 3)) and twice with PBS. Then cells were fixed for 30 min in 4% paraformaldehyde at 37 °C and washed with PBS for another three times. Coverslips were inverted, Fluoromount added, and dried overnight. Fluorescently labeled rMIF, labeled with carboxyfluorescein using a kit from Roche Diagnostics as described previously (14), was used for comparison and to establish the endocytosis assay in the fibroblast cell line. Cell-bound fluorescence was scored by fluorescence microscopy and quantitated with the Soft Imaging Systems software (Münster, Germany).

RESULTS

Design, Synthesis, Purification, and Chemical Properties of MIF-(50–65) and Its Derivatives—Small peptide derivatives of TPORs containing as few as 6 residues have been reported to retain some of the redox and biochemical properties of their parent protein molecules (35, 36). Election of peptide fragment 50–65 of the cytokine MIF (the nomenclature refers to the

cDNA sequence of human MIF with the Met-1 residue constituting amino acid number 1 of the MIF sequence and does not take into account that Met-1 is post-translationally processed) as a potentially minimized MIF derivative was based on peptide sequence MIF-(56–65), which had been shown previously to exhibit low but measurable MIF-like catalytic oxidoreductase activity (19). MIF-(50–65) also spanned the C*XX*C motif of human MIF and encompassed the β4-strand. Other than MIF-(56–65), which covered the β4-strand only, MIF-(50–65) was chosen to include additional residues that could serve to stabilize secondary structure interactions. In fact, it has been proposed for the TPORs that formation of a stable β-turn structure in the C*XX*C region is associated with oxidoreductase activity (37). Therefore, MIF-(56–65) was N-terminally extended up to residue Phe-50 to enable formation of additional intramolecular C*XX*C structure-stabilizing interactions. At the same time, this meant that MIF-(50–65) encompassed the extended TPOR motif according to Ellis *et al.* (16), which included the Phe residue at position 50. Initial secondary structure predictions by the methods of Chou and Fasman (53) and Garnier *et al.* (54) indicated that sequence 50–65 had a reasonably high β-turn-forming probability of up to 37.5% and was sufficiently long to form a stable intramolecular β-sheet structure (55). Downstream of the C*XX*C motif, the sequence covered the residues up to position 65 to contain two Ser residues and His-63. These residues as well as the two serines lying upstream of C*XX*C were deemed potentially important due to their principal capability of stabilizing the cysteine thiolate or generating a dipole function (56). Also, MIF-(50–65) contained an inverse C*XX*S motif (corresponding to residues 57 → 54). C*XX*S groups have been recognized recently as fold independent redox motifs that are indicative of TPORs (57).

As a potentially inactive derivative of MIF-(50–65), C57S/C60S-bis-serine-MIF-(50–65) was chosen, whereas biotinylated MIF-(50–65) and biotin-C57S/C60S-MIF-(50–65), which were devised for binding assays, were designed to carry N-terminal biotinylation with an aminocaproate group as a spacer to minimally interfere with the conformation of the peptide. For cell uptake studies, fluorescent peptides were synthesized with a carboxyfluorescein moiety linked to the N terminus. To probe further the conformational changes of MIF-(50–65) that were expected to occur upon intramolecular disulfide formation, the covalently cyclized analog of MIF-(50–65), cyclo^{57,60}-[Asp^{57},Dap^{60}]MIF-(50–65) (abbreviated as cyclo-MIF-(50–65)) and its corresponding linear control peptide [Asp^{57},Dap^{60}]MIF-(50–65) were applied. The sequences of the peptides are shown in Fig. 1*A*.

SPPS gave the peptides in good yield. Crude products of the syntheses except for that of the fluoresceinated bis-serine variant consisted of the desired product to a degree more than 90%. The crude product of Fluo-C57S/C60S-MIF-(50–65) contained a significant fraction of a synthesis side product that was removed by an additional interim RP-HPLC step. Together, using RP-HPLC purification, all peptides were obtained in their reduced forms at purities greater than 98% (Fig. 1, *B–E*). The obtained M + 1 masses of the products were in good agreement with the theoretical mass values (measured mass of MIF-(50–65) = 1648.9 Da, expected, 1648.9 Da; measured mass of C57S/C60S-bis-serine-MIF-(50–65) = 1617.0 Da, theoretical, 1617.8 Da; measured mass of biotin-Aca-MIF-(50–65) = 1945.8 Da, expected, 1945.3 Da; measured mass of biotin-Aca-C57S/C60S-MIF-(50–65) = 1914.6 Da, expected, 1915.2 Da; measured mass of Fluo-MIF-(50–65) = 1964.4 Da, expected, 1964.1 Da; Fluo-C57S/C60S-MIF-(50–65) = 1934.8 Da, expected, 1934.0 Da; measured mass of cyclo^{57,60}-[Asp^{57},Dap^{60}]MIF-(50–65) = 1625.4 Da; expected: 1626.8 Da; measured mass of [Asp^{57},Dap^{60}]MIF-(50–65) = 1643.3 Da; expected, 1643.8 Da).

Incubation of MIF-(50–65) with an excess of DTT led to a rapid and complete reduction of MIF-(50–65). Fig. 1*F* shows the HPLC elution profile of oxidized *versus* reduced MIF-(50–65) with the reduced species eluting 0.7 min earlier than the oxidized peptide. The HPLC procedure and elution profile was highly reproducible and was thus also used for the generation of the reduced and oxidized species of MIF-(50–65) at a preparative scale. Under these reducing conditions, no intermediate mixed disulfide species were observed. Mass spectrometric analysis using either liquid chromatography-coupled electrospray MS or MALDI-TOF-MS showed the expected mass difference of 2 Da between the species, with oxidized MIF-(50–65) having a M + 1 mass of 1646.7 Da (theoretical M + 1 mass = 1646.9 Da) and reduced MIF-(50–65) having a M + 1 mass of 1649.0 Da (theoretical M + 1 mass = 1648.9 (Fig. 1, *G* and *H*). Of note, the oxidized and reduced species of full-length MIF eluted in the same order from the C18 HPLC column (reduced rMIF, 17.56 ± 0.44 min, $n = 5$; oxidized rMIF, 17.85 ± 0.34 min, $n = 5$). On the other hand, the shorter MIF fragment, MIF-(56–65) showed an inverse elution profile, with the oxidized species eluting 0.6 min before the reduced one. Thus, although the differences in elution time observed for the full-length MIF species were not significant ($p > 0.05$), this indicated that MIF-(50–65) was similar to rMIF with respect to the conformational changes and subsequent changes in molecular surface hydrophobicity that occur during oxidation/reduction.

Disulfide-dependent β-Turn Formation of MIF-(50–65)—CD spectropolarimetry was applied to estimate the conformational properties of MIF-(50–65). Near-UV CD analysis confirmed intramolecular disulfide formation of MIF-(50–65) following air oxidation of the peptide. Oxidized MIF-(50–65) showed a CD signal between 270 and 285 nm that is characteristic of a disulfide group and that was not detectable when the reduced peptide or the bis-serine derivative were analyzed by near-UV CD (Fig. 2*A*). Oxidation-induced disulfide formation was reversible. When oxidized MIF-(50–65) was incubated with DTT for a period from 10 min to 24 h, the CD signal at 270–285 nm decreased successively (Fig. 2*B*). After 24 h of reduction, the spectrum was superimposable to that of fully reduced MIF-(50–65). The kinetics of the reduction process indicated that the peptide can readily undergo oxidation/reduction processes.

The far-UV CD spectra of reduced MIF-(50–65) and C57S/C60S-MIF-(50–65) exhibited strong minima at about 200 nm which indicated that both peptides were predominantly unordered, with C57S/C60S-MIF-(50–65) being significantly more unordered than MIF-(50–65). Disulfide formation of MIF-(50–65) was accompanied by a clear increase in β-turn structure. Fig. 2*C* shows that the far-UV CD spectrum of oxidized MIF-(50–65) exhibited a well pronounced minimum at 225–230 nm (58). By contrast, reduced MIF-(50–65) and the bis-serine mutant did not exhibit significant minima in this wavelength range. This indicated that formation of the disulfide bridge in MIF-(50–65) was associated with β-turn stabilization. The magnitude of the random coil minimum and thus of random coil content was significantly reduced in oxidized MIF-(50–65) as compared with reduced MIF-(50–65) which indicated that β-turn stabilization was associated with an increase in conformational ordering of this molecule. Of note, disulfide formation-induced β-turn stabilization of MIF-(50–65) was further confirmed by CD analysis of cyclo-MIF-(50–65). This peptide analog of MIF-(50–65) contained a covalent side chain-to-side chain lactam bridge between residues 57 and 60 which had been substituted by Asp and Dap, respectively. The ring struc-

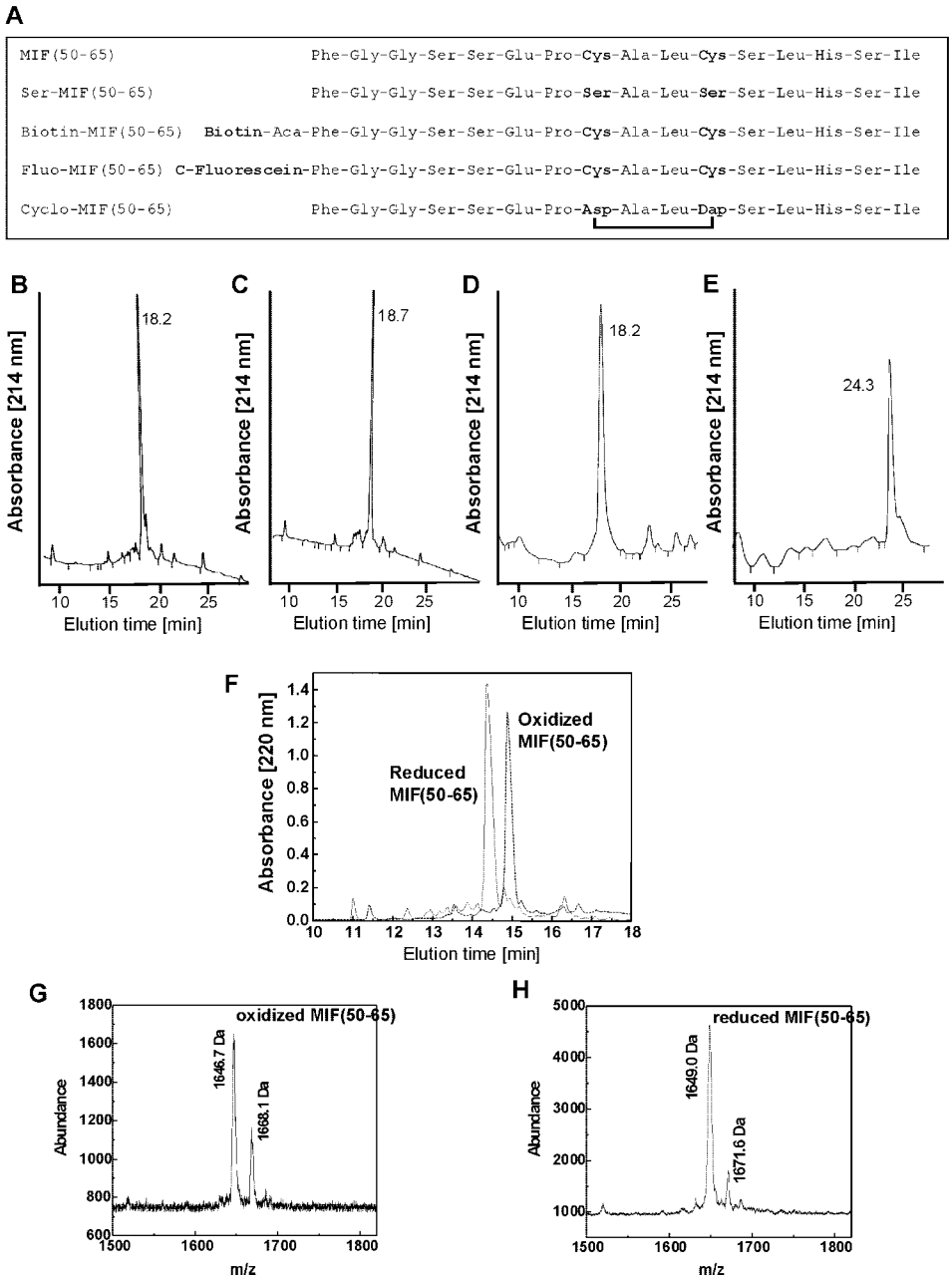

FIG. 1. **Design and synthesis of peptide fragment MIF-(50–65) of human MIF.** *A*, amino acid sequences of MIF-(50–65), the bis-serine variant of MIF-(50–65) (Ser-MIF-(50–65)), biotinylated MIF-(50–65), fluoresceinated MIF-(50–65), and side chain-to-side chain cyclized MIF-(50–65). Numbering refers to the cDNA sequence. The cysteine and serine residues of the C*XX*C motif, the biotin group, the carboxy-fluorescein group, and the cyclic constraint are shown in *boldface*. *B–E*, MIF-(50–65) and its derivatives were obtained in good yield and purity by Fmoc solid phase peptide synthesis. C18 reverse phase HPLCs (see "Materials and Methods") of the crude synthesis products of MIF-(50–65) (*B*), the bis-serine mutant (*C*), and biotinylated MIF-(50–65) (*D*) are shown. The HPLC of cyclo-MIF-(50–65) (*E*) was recorded after removing a synthesis side product by an interim HPLC step. The elution time is plotted over the absorbance at 214 nm. *F*, separation of oxidized MIF-(50–65) from reduced MIF-(50–65). Purified air-oxidized MIF-(50–65) can be well resolved from DTT-reduced MIF-(50–65) by analytical C18 HPLC. The elution time is plotted over the absorbance at 220 nm. *G* and *H,* MALDI-TOF-MS spectra of purified air-oxidized and purified DTT-reduced MIF-(50–65). In addition to the M + 1 peaks, the sodium adducts of the peptides (M + 23) were observed.

ture in this cyclic analog had the same size as the ring structure that was formed in the disulfide-bridged oxidized form of MIF-(50–65). The CD spectrum of this analog exhibited a pronounced minimum at 225 nm that was even stronger than that for oxidized MIF-(50–65), indicating that the cyclic structure resulted in significant β-turn stabilization (Fig. 2*D*). By contrast, the corresponding linear control peptide [Asp^{57},Dap^{60}]MIF-(50–65) had no minimum at this wavelength but was rather predominant in a random coil conformation as evidenced by a marked minimum at 200 nm (Fig. 2*D*). Thus, the far-UV CD spectrum of cyclo^{57,60}-[Asp^{57},Dap^{60}]MIF-(50–65) was similar to that of oxidized MIF-(50–65), whereas the spectrum of [Asp^{57},Dap^{60}]MIF-(50–65) was most similar to that of C57S/C60S-MIF-(50–65).

Thiol/Disulfide Equilibrium Measurements, Mixed Disulfide Formation, and Redox Potential of MIF-(50–65)—We next were interested in investigating the redox properties of MIF-(50–65) in more detail. This encompassed equilibrium measurements and determination of the redox potential of the peptide. Redox equilibrium measurements were performed with both glutathione (GSH/GSSG) and cysteine/cystine as reference redox pairs. Both references were applied in excess over MIF-(50–65). Reactions were quenched, and the distribution of

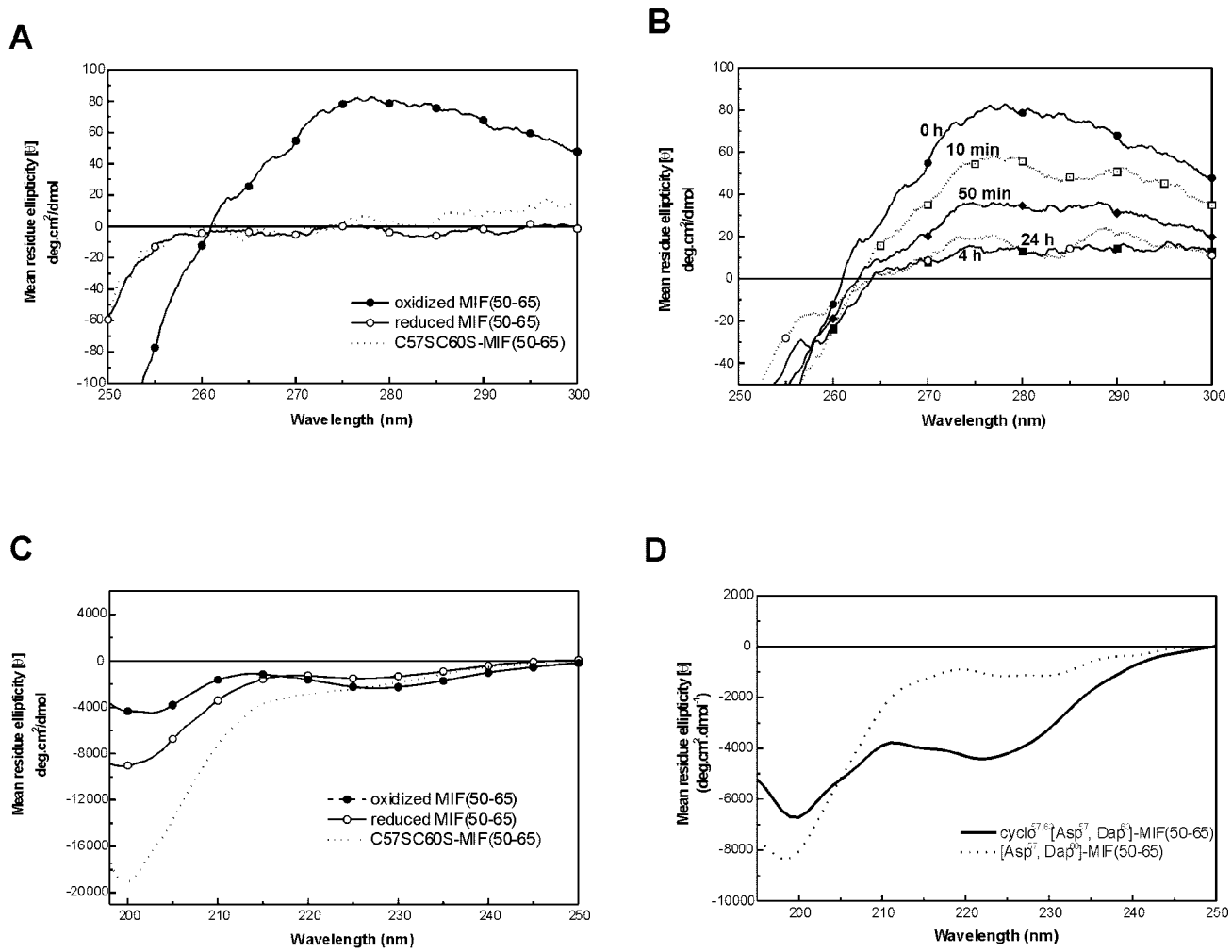

FIG. 2. **Near and far-ultraviolet CD spectroscopy indicated disulfide-dependent cyclization and β-turn formation of MIF-(50–65).** *A*, disulfide formation of MIF-(50–65) following oxidation was shown by comparison of the near-UV CD spectra of oxidized MIF-(50–65) with those of DTT-reduced MIF-(50–65) and the bis-serine mutant. The strong absorption maximum between 270 and 285 nm is indicative of disulfide bond formation. *B*, near-UV CD spectra of the kinetics of reduction of oxidized MIF-(50–65) with DTT. Oxidized MIF-(50–65) was completely reduced by DTT within 4 h. Oxidation and disulfide formation was fully reversible. *C*, far-UV CD spectroscopy showed that upon oxidation and disulfide formation, MIF-(50–65) was conformationally stabilized as indicated by a decrease in the portion of random coil and by the formation of a minimum at 225–230 nm. The latter indicated formation of a β-turn structural element. The bis-serine mutant was analyzed for control. *D*, far-UV CD spectroscopy of the cyclic analog cyclo^{57,60}-[Asp^{57},Dap^{60}]MIF-(50–65) and comparison with the spectrum of the linear control peptide [Asp^{57},Dap^{60}]MIF-(50–65). The cyclic analog shows a strong minimum at 225 nm, indicating marked β-turn stabilization. CD spectra are plotted as the mean residue ellipticity [θ] in degrees·cm^2/dmol over the wavelength in nm.

the peptide species was analyzed by quantitative RP-HPLC and, in some experiments, by mass spectrometric analysis.

Preliminary experiments were performed with GSH/GSSG, using ratios of 50/10, 50/1, and 50/0.001. At a ratio of 50/1, most of the oxidized peptide (elution time, 14.9 min) was converted into the reduced form (14.2 min) within 2 h of reduction. However, this analysis also indicated that several peaks with shorter elution times appeared. By using a ratio of 50/0.001, essentially the entire amount of oxidized peptide was reduced within 2 h with no additional peaks observed. By using a ratio of 50/10, only a small portion of the oxidized peptide was reduced in 2 h, and also after 48 h, additional strong peaks were seen, indicating that stable mixed disulfides may have formed (data not shown).

Equilibrium and redox potential measurements were then performed at a fixed total concentration of GSH/GSSG or cysteine/cystine of 50 mM. Mixed disulfide formation was measured at a ratio of 42/8, incubating the mixtures for 20 h. Under these conditions, a similar chromatogram containing additional peaks indicative of mixed disulfide species was obtained as for the 50/10 ratio in the scouting experiments (Fig. 3*A*). Kinetic studies (Fig. 3*B*) showed on the one hand that equilibrium was reached at 20 h, as no changes in the chromatogram were observed toward 42 h and, on the other hand, indicated that a mixed disulfide species peak at an elution time of 13.4 min appeared as early as 10 min after starting the reaction. Another potential mixed disulfide peak was observed at 30 min and had an elution time of 12.4 min. Both peak intensities as well as that of oxidized peptide declined over time as the peak of reduced MIF-(50–65) increased.

The identity of the potential mixed disulfide species was studied by MALDI-TOF-MS of the collected peak fractions at equilibrium conditions. Table I summarizes the obtained masses and their assignments. The equilibrium mixture contained a significant portion of mono-mixed disulfide (GS-S-MIF-(50–65)) (~30%) and ~10% of the di-mixed disulfide species (GS-S-MIF-(50–65)-S-SG). Less than 2% MIF-(50–65) dimer was measured, confirming preliminary prior data that covalent dimerization is not favored for either MIF or MIF-derived C*XX*C-spanning peptides. Only one mono-mixed disulfide species could be detected. It is unclear whether only one mono-mixed species formed, whether one species was unstable,

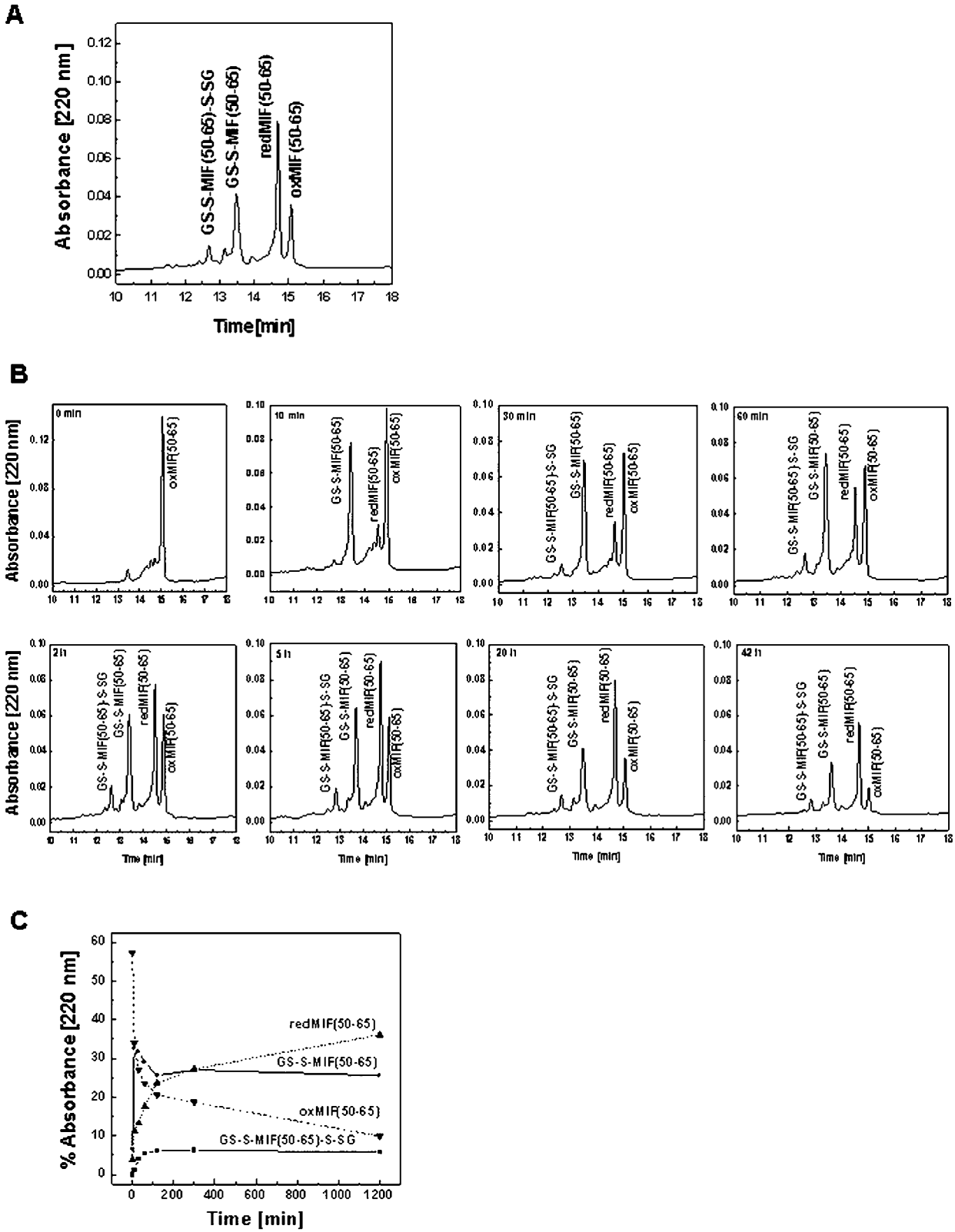

FIG. 3. **Thiol/disulfide equilibrium studies of MIF-(50–65) with the GSH/GSSG redox reference pair and evidence for stable mixed disulfide formation.** Reactions were analyzed by analytical C18 HPLC. *A*, equilibrium mixtures (20 h) of purified oxidized MIF-(50–65) with a molar excess of GSH/GSSG at ratio of 42/8 mM indicated that a stable mono-mixed disulfide and stable di-mixed disulfides had formed and that reduced MIF-(50–65) was the predominant species at equilibrium. The second mono-mixed disulfide species could not be detected. *B*, kinetics of the reduction and formation of mixed disulfides in mixtures of oxidized MIF-(50–65) with GSH/GSSG (42/8 mM). Reactions from 0 min to 42 h were quenched with 1 M H_3PO_4, and chromatograms were recorded as described under "Materials and Methods." *C* summarizes the chromatograms of *B*. A mono-mixed disulfide species formed early on and was prominent at 10 min, indicating that it was a transition state for the formation of reduced MIF-(50–65). Detectable from 30 min on, an apparently stable di-mixed disulfide species formed. The relative reduction of the percentage of mono-mixed disulfide species between 30 min and 5 h indicated that this species was a transition state for reduced MIF-(50–65). Changes in absorbance between 20 and 42 h were not significant; equilibrium was reached at around 20 h. Chromatograms represent the elution times of the peptide species plotted over the absorbance at 220 nm.

TABLE I
Mass spectrometric measurements of oxidized and reduced MIF(50–65) and the isolated mixed glutathione-MIF peptide species

Species	Relative abundance at equilibrium	Retention time	Expected M + Na^+ mass for species	Experimentally determined M + Na^+ mass
	%	*min*		*Da*
oxMIF (50–65)	18	14.9	1668	1669.0
redMIF (50–65)	40	14.4	1670	1670.7
mono-mixed disulfide (GS-S-MIF (50–65))	30	13.5	1976	1976.5
Dl-mixed disulfide (GS-S-MIF (50–65)-S-SG)	10	12.4	2281.6	2281.3
Dimer	<2	6	3292 Da[a]	3295.1[a]

[a] M + H^+ mass; equilibrium mixtures were quenched with phosphoric acid and fractionated by C18 HPLC as described under "Materials and Methods." Peaks of the indicated elution times were collected, immediately frozen on dry ice, lyophilized, and analyzed by MALDI-TOF-mass spectrometry. Only one mono-mixed disulfide species could be detected.

or whether the elution times of both species were very similar such that the peaks could not be resolved. Fig. 3*C* summarizes the kinetics of the reduction reaction.

Initial measurements with cysteine/cystine at a ratio of 42/8 indicated that the reduction process was much faster than when the GSH/GSSG redox pair was used. After 10 min, reduced MIF-(50–65) represented already ~60% of total peptide. For comparison, at this time point only <5% of peptide were in the fully reduced state when the glutathione mixture was applied (see Fig. 3*B*). Equilibrium was reached already at 5 h (Fig. 4*A*). A detailed kinetic analysis of the cysteine-dependent reduction between 0 and 10 min then demonstrated that a marked portion of reduced MIF-(50–65) was already detectable at 2 min (~30%). By 10 min, reduced MIF-(50–65) was the predominant species present (see above). Mixed disulfide formation was fast and transient, with only small peaks (~5% each) with elution times of 13.5 and 12.5 min observed at 2 min, which further declined in intensity toward 10 min (Fig. 4*B*).

The redox potential E'_0 of MIF-(50–65) was determined at equilibrium using various ratios of GSH/GSSG and cysteine/cystine. The detectable peptide species were quantitated by HPLC and the relative abundance of the peak areas used to determine K_{ox}, which in turn was used to calculate E'_0 through the Nernst equation (see "Materials and Methods"). By using GSH/GSSG as a reference redox pair, a E'_0 value of −0.258 V was obtained. Applying cysteine/cystine, E'_0 was found to have a value of −0.255 V. The latter result confirmed that the calculation of K_{ox} can be based on the two-state model. Together, these measurements showed that the redox potential of MIF-(50–65) was a strongly negative one.

MIF-(50–65) Has Catalytic Oxidoreductase Activity in Vitro—MIF was shown to exhibit thiol-protein oxidoreductase activity in the insulin reduction and HED transhydrogenase assay (19). Here we demonstrated that MIF-(50–65), at a 10-fold higher concentration than full-length rMIF, was able to catalyze insulin reduction. This activity was dependent on the presence of the C*XX*C cysteine residues as the bis-serine mutant peptide was inactive (Fig. 5*A*). MIF-(50–65) also catalyzed the reduction of 2-HED, although this activity was very low (only 17% of rMIF at a 10-fold higher concentration) and not significant (data not shown). As expected from previous structure activity relationship studies on the oxidoreductase and tautomerase activities of MIF (23), MIF-(50–65) did not catalyze the conversion of D-dopachrome methyl ester, whereas full-length rMIF potently catalyzed this reaction (Fig. 5*B*).

Thus, these findings confirmed the notion that the TPOR activity of MIF is mediated by a sequence stretch around the C*XX*C motif. As for other TPORs, MIF-derived C*XX*C-spanning peptide fragments appear to bear some of the catalytic TPOR activity of the full-length protein. The result also confirmed previous notions that the TPOR and tautomerase activities of MIF are mediated by distinct regions of the MIF molecule (23, 59).

MIF-(50–65) Exhibits MIF-like Immunostimulatory Activities—The immunostimulatory activity of MIF has been best characterized by the capacity of MIF to override the antiinflammatory and immunosuppressive activity of glucocorticoids (3). The glucocorticoid antagonistic activity of MIF is unique among cytokines and has been shown to be relevant *in vivo* (3, 60). A C*XX*C mutant of MIF was found to have significantly reduced glucocorticoid overriding (GCOR) activity compared with the wild-type protein, indicating that the TPOR activity could be important for GCOR. We therefore hypothesized that, in addition to exhibiting oxidoreductase activity, MIF-(50–65) may have MIF-like GCOR activity. When testing overriding of the suppression by DEX of TNF secretion from LPS-stimulated THP-1 monocytes, MIF-(50–65) was in fact found to have GCOR activity. At a concentration of 3.3 μM, MIF-(50–65) led to an overriding of ~45%. Lower concentrations of 1 μM and 50 nM had no activity. The activity of 3.3 μM MIF-(50–65) was comparable with that obtained for 0.16 nM rMIF (Fig. 6*A*). The bis-serine variant did not show any GCOR activity at any of the concentrations tested (50 nM to 3.3 μM). Thus, although the concentration of the peptide needed was much higher than for full-length MIF, we concluded that the 16-meric MIF peptide had at least partial MIF-like immunologic activity.

Protein minimization has been attempted for several cytokines and hormones and has only been successful in some cases (see "Discussion"). Thus, to confirm whether MIF-(50–65) exhibited an immuno-stimulatory potential characteristic of MIF, we tested cellular activation by the peptide in several other experimental settings.

MIF has been shown to modulate the proliferation of a number of different cell types. For example, a potent proliferative activity of MIF has been described in fibroblasts (13). We found that MIF modulated the proliferation of primary vascular endothelial cells. Proliferation-modulating effects of MIF were observed for both human microvascular endothelial cells (MVEC) and human umbilical vein endothelial cells (latter not shown). Regulation of the cellular activation state of endothelial cells by MIF could be important for MIF-mediated inflammatory reactions in human atherogenesis (15). We show that rMIF enhanced the proliferation-inducing effect of bFGF and VEGF on MVEC in a concentration-dependent manner (Fig. 6, *B* and *C*). Significant induction of proliferation by MIF was observed for MIF concentrations ranging from 8 to 400 nM. Importantly, the activity measured was based on the use of an assay with primary cells rather than immortal cell lines. It was therefore tested whether MIF-(50–65) exhibited MIF-like activity in this assay. We found that MIF-(50–65), like MIF, enhanced the inducing effects of both bFGF and VEGF on MVEC proliferation in a concentration-dependent manner. Significant proliferation-stimulating activity was observed at concentrations over 1 μM. The bis-serine variant of MIF-(50–65) had no significant activity (Fig. 6, *B* and *C*).

MIF-(50–65) Modulates Intracellular Signaling Targets of MIF—We next asked whether the 16-meric peptide analog was also capable of modulating intracellular pathways in a MIF-

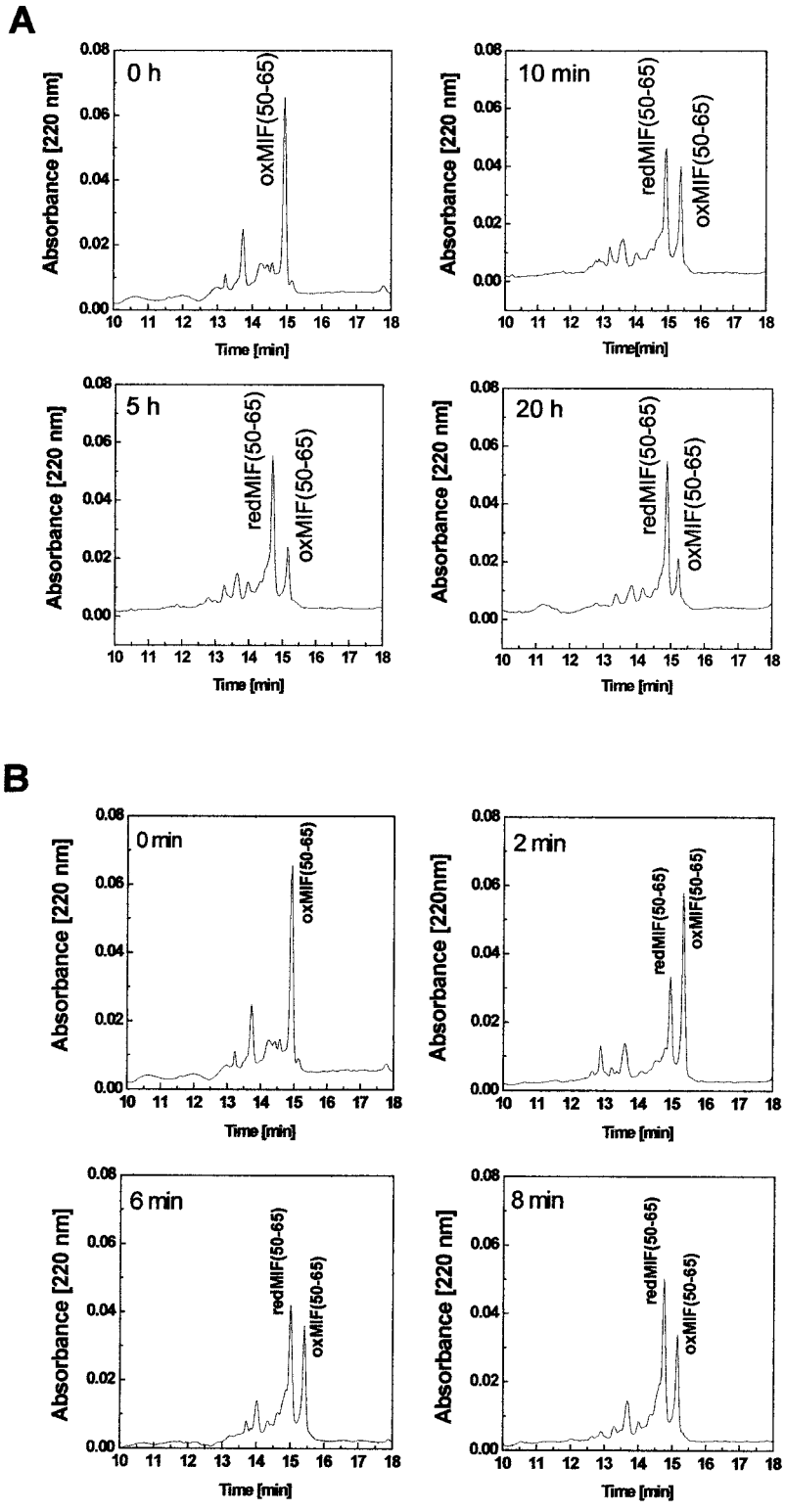

FIG. 4. **Thiol/disulfide equilibrium studies of MIF-(50–65) with the cysteine/cystine redox reference pair.** Mixed disulfide formation occurred immediately after mixing the components and appeared to be transient only. Reactions were analyzed by analytical C18 HPLC. *A*, time course of thiol/disulfide exchange reactions (cysteine/cystine ratio of 42/8 mM) from 0–20 h. No change in elution profile was observed after 5 h. *B*, time course between 0 and 8 min. Peak representing substantial amounts of mixed disulfide species were not observed even at 2 min. Chromatograms were recorded as described under "Materials and Methods" and represent the elution times of the peptide species plotted over the absorbance at 220 nm.

like manner. As activation of the ERK1/2 kinase had been linked to the proliferation-stimulating effect of MIF (13), we first investigated the effect of the peptide on the formation of intracellular endogenous phospho-ERK1/2 levels in NIH 3T3 fibroblasts. In initial experiments, we confirmed the reported stimulatory effect of rMIF on ERK1/2 activity in these fibroblasts (Fig. 7*A*, *right panel*). We then compared the effect of MIF with the potential effect of MIF-(50–65). Because we wanted to later on probe whether MIF-(50–65) could bind to the cellular binding partner of MIF, JAB1, and biotinylated MIF-(50–65) was to be used for the binding studies, we applied both biotinylated MIF-(50–65) and MIF-(50–65) in the ERK1/2 phosphorylation experiments and included the corresponding bis-serine MIF-(50–65) peptides for comparison. Both biotin-MIF-(50–65) (Fig. 7*A*, *top panel*) and MIF-(50–65) (Fig. 7*B*, *middle panel*) stimulated the phosphorylation of ERK1/2. Induction of the phosphorylation of ERK1/2 by the peptide was concentration-dependent, with the maximal induction observed at 330 nM and with some effect already observed at concentrations as low as 3 nM peptide. The activity of MIF-

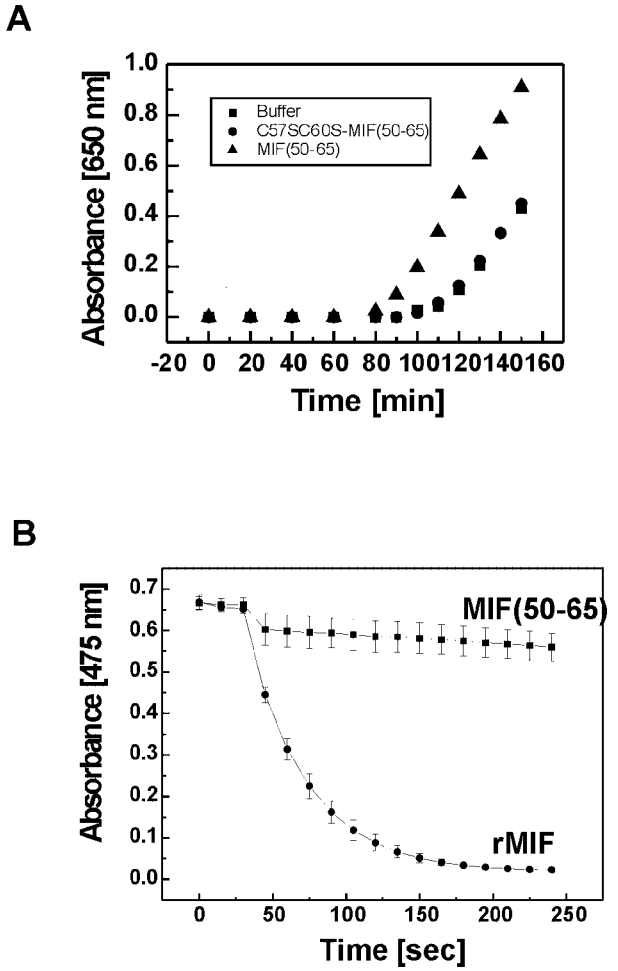

FIG. 5. **MIF-(50–65) exhibits catalytic thiol-protein oxidoreductase but no D-dopachrome tautomerase activity.** *A*, MIF-(50–65) but not C57S/C60S-MIF-(50–65) reduces insulin disulfides. The catalytic activity was measured in a turbidometric assay that relied on the insolubilization of the insulin B-chain following disulfide reduction using glutathione as a cofactor as described under "Materials and Methods." The absorbance at 650 nm representing light scattering by B-chain aggregates is plotted over the reaction time. *B*, MIF-(50–65) does not share with full-length human MIF the ability to catalyze the conversion of D-dopachrome methyl ester. The plot shows the absorbance at 475 nm *versus* the reaction. The assay is described in detail under "Materials and Methods."

(50–65) was ~1000-fold higher than that of the bis-serine control peptide, as this peptide exhibited only minor activity at 3.3 μM (Fig. 7*A*, *middle panel*). Thus, MIF-(50–65) was able to stimulate specifically the ERK1/2 MAPK pathway that is activated by MIF in fibroblasts. A first indication as to the mechanism of ERK1/2 activation was obtained by testing the cyclo-MIF-(50–65) in comparison with a linear control peptide. The analysis showed (Fig. 7*A*, *lower panel*) that this non-cysteine-containing, β-turn-stabilized MIF-(50–65) analog stimulated ERK phosphorylation comparable with MIF-(50–65), confirming the importance of the presence of a β-turn conformation for triggering this signal transduction process (see "Discussion" for an initial mechanistic model).

JAB1/CSN5 has been shown to be an intracellular binding partner of MIF. MIF can modulate intracellular signaling pathways through JAB1, which has been one of the few characterized signaling targets of MIF (14). It was therefore of interest if the MIF-derived peptide was able to bind directly to JAB1. Biotinylated MIF-(50–65) was applied to probe for complex formation between radioactively labeled JAB1 and the peptide by pull-down assay. Fig. 7*B* shows that MIF-(50–65) specifically bound to JAB1. This finding was thus in line with previous observations that MIF-(50–65) could compete with MIF for JAB1 binding (14). Complex formation between biotin-MIF-(50–65) and JAB1 was further confirmed by pull-down of complexes of biotin-MIF-(50–65) and the so-called MPN domain of JAB1. In this setting, complexes of biotin-MIF-(50–65) and *in vitro* translated MPN protein were precipitated by newly developed streptavidin-conjugated nanoparticles and MPN directly measured by MALDI-TOF-MS from surface-immobilized streptavidin nanoparticle (data not shown; to be published in detail elsewhere). Interestingly, the bis-serine derivative of MIF-(50–65) also bound to JAB1. This finding was also in agreement with prior competition experiments that had shown that the serine variant also interfered with MIF binding to JAB1. Together, these data indicated that the sequence stretch 50–65 was sufficient for the binding of MIF to JAB1. They also indicated that the C*XX*C cysteine residues were dispensable for binding.

Because in the cellular activation assays (GCOR, proliferation, and ERK1/2 kinase assay), the bis-serine variant of the peptide was essentially inactive, we wished to compare the effects of the two peptides with respect to cellular targets/activities which MIF can regulate in a JAB1-dependent manner. As MIF had been demonstrated to stabilize $p27^{Kip1}$ levels in a JAB1-mediated way, we studied the effect of MIF-(50–65) on cellular p27 levels and compared the effect to that of full-length rMIF and C57S/C60S-MIF-(50–65). Fig. 7*C* shows that MIF-(50–65) had a comparable p27 concentration-enhancing effect as rMIF. The effect was concentration-dependent with a maximum induction measured at peptide concentrations of 2–3 μM. As seen in the JAB1 binding experiments, the bis-serine variant exhibited a similar activity. In conjunction with the result of the binding study, this indicated that sequence stretch 50–65 is important and sufficient for JAB1 binding and modulation of at least some of the JAB1 activities by MIF. By contrast for the GCOR, cell proliferation-stimulating and MAPK activity assays, the presence of the C*XX*C cysteine residues and/or β-turn conformation appeared to be critical.

MIF-(50–65) and the Bis-serine Peptide Are Endocytosed by MIF Target Cells at a Similar Rate—Binding to JAB1 and modulation of p27 levels by the peptides suggested that both MIF-(50–65) and the bis-serine analog can be taken up by MIF target cells to then act intracellularly. We thus confirmed that the peptides, like MIF, were endocytosed by NIH 3T3 cells. Fluorescently labeled MIF-(50–65) and C57S/C60S-MIF-(50–65) were both found to be endocytosed by the fibroblasts within 60 min (Fig. 8 and data not shown). However, uptake of the peptides was less efficient than that for fluorescently labeled rMIF (Fig. 8*A*), for which marked cell-bound fluorescence was already seen after 10 min (latter not shown). Because the bis-serine variant of MIF-(50–65) was essentially inactive in the GCOR, proliferation, and ERK assays, but exhibited MIF-like activity on the putative intracellular MIF signaling targets JAB1 and p27, it appeared important to compare directly the endocytosis efficiency of MIF-(50–65) and the bis-serine variant. Quantification of the cell-bound fluorescence for the two peptides showed that the two peptide species were endocytosed at a similar rate (Fig. 8*B*). This suggested that different activity profiles observed for the peptide species in the various activity assays were not due to differences in their cellular uptake rates. The higher uptake rate of rMIF as compared with the peptides may in part be due to the higher labeling grade of rMIF (14) but may also indicate that MIF but not the peptides could recruit additional proteins to facilitate uptake and signaling.

Together, the immunological and cellular activation assays

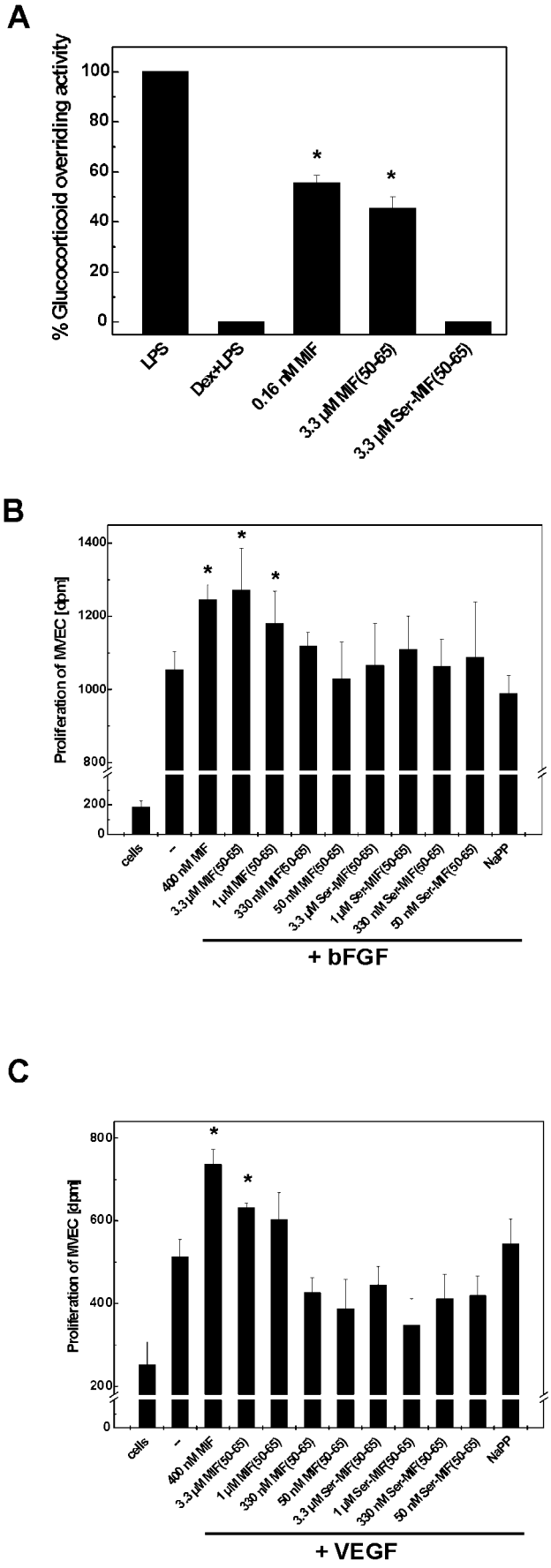

FIG. 6. **Analyses in the GCOR assay and a cell proliferation assay show that MIF-(50–65) exhibits typical MIF-like immunostimulatory activities.** *A*, MIF-(50–65) but not C57S/C60S-MIF-(50–65) has GCOR activity as demonstrated in a THP-1 monocyte-based overriding assay (see "Materials and Methods"). The activity of MIF-(50–65) and its bis-serine variant was compared with the activity of full-length human MIF. Lower concentrations of MIF-(50–65) did not exhibit any GCOR activity. Percent GCOR activity is plotted, whereby 100% overriding was defined as that amount of secreted TNF that was induced by LPS. Suppression of LPS-induced TNF by 10^{-6} M dexamethasone (DEX, Dex) represented 0% overriding activity. *Asterisks* indicate statistically significant values ($p < 0.05$) in comparison to the "DEX + LPS value" as determined by unpaired Student's *t* test. Values represent the mean ± S.D. of 3–18 measurements. *B* and *C*, MIF-(50–65) but not C57S/C60S-MIF-(50–65) enhances the bFGF-induced (*B*) and VEGF-induced (*C*) proliferation of microvascular endothelial cells (MVECs) comparable with full-length human MIF. The effect of various peptide concentrations was compared with that of 400 nM full-length MIF. Control cells were not treated at all (*cells*), incubated with growth factor alone (−), or incubated with the same volume of phosphate buffer as that used for the peptide incubations (*NaPP*). *Asterisks* indicate statistically significant bars ($p < 0.05$ according to the unpaired *t* test) with respect to the "cells + growth factor alone (−)" bars. *Bars* represent the mean ± S.D. of 3 measurements. Proliferation of MVECs is plotted as incorporated radiolabeled thymidine in dpm values.

demonstrated that MIF-(50–65) not only shared with MIF its oxidoreductase activity *in vitro* but also had the intriguing capacity to modulate cellular activation in a MIF-like fashion. Comparison of MIF-(50–65) with its bis-serine variant and side chain-to-side chain cyclized analog and application of MIF assays representing different signaling pathways, provided important mechanistic information as to the molecular interaction of MIF and the peptides with MIF target molecules.

DISCUSSION

MIF is a relatively small protein mediator, for which numerous biological activities have been demonstrated. Due to its potent inflammation- and immuno-regulatory properties, MIF has mostly been viewed as a cytokine, although endocrine-like functions have been described and although MIF differs from typical cytokines with respect to several characteristics (reviewed in Refs. 5 and 6). A membrane receptor that could serve to mediate the various activities of MIF has not yet been identified, whereas two intracellular proteins, the transcriptional co-activator JAB1 (14) and peroxiredoxin (24), have been shown to bind to MIF. Functional analysis indicated that JAB1 activity is antagonized by MIF (14). Nevertheless, as MIF triggers certain other typical signal transduction pathways such as the ERK1/2 MAPK pathway, it is likely that some of the functions of MIF are funneled through receptor-mediated pathways.

In addition, two distinct catalytic activities, *i.e.* a TPOR and a dopachrome isomerase activity, have been described for MIF (19, 48). These activities have clearly been demonstrated in *in vitro* studies, but their physiological role has remained open. Consisting of only 114 residues, it is not surprising that for MIF, no typical domain structure has been identified. However, previous structure activity studies have indicated that the catalytic activities of MIF reside within small sequence motifs (23, 61). The TPOR activity is mediated by a C*XX*C sequence in the middle of the MIF molecule, whereas the isomerase activity is dependent on an N-terminal Pro residue. In line with the latter finding, MIF-(50–65) did not show any D-dopachrome tautomerase activity. The TPOR activity is further enhanced by N-terminal residues (23), whereas for the tautomerase function, C-terminal residues and additional other residues critically participate in forming the substrate pocket (59, 62).

Our previous studies on N-terminally truncated MIF mutants indicated that for certain typical MIF activities the N-terminal region of the molecule is dispensable (23). However, these prior minimization attempts only led to MIF derivatives with truncations of less than 10 residues. Also, C-terminally

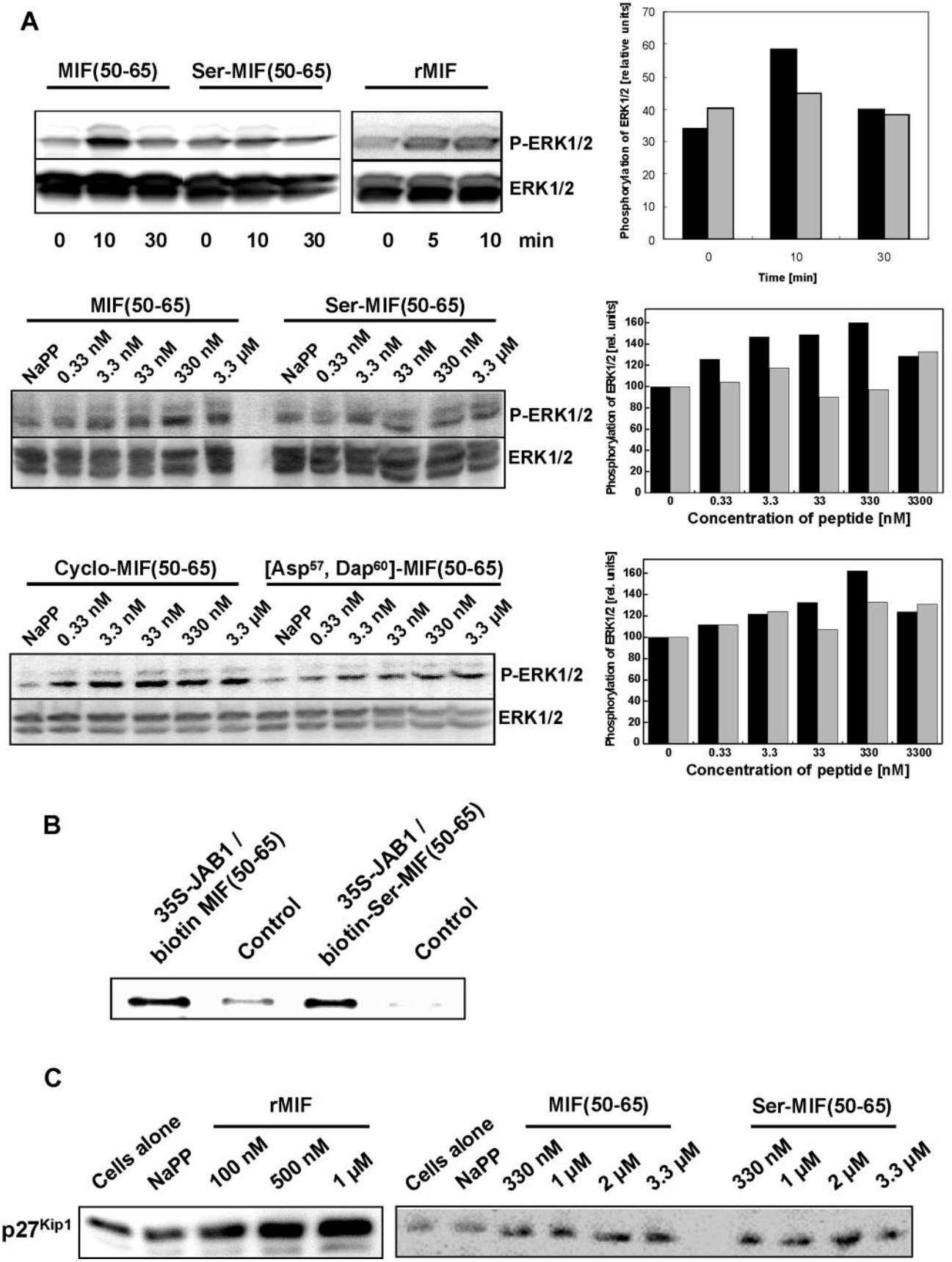

FIG. 7. **MIF-(50–65) modulates signal transduction processes in a MIF-like fashion.** *A*, concomitant with the growth-stimulatory effect of MIF-(50–65) as seen in Fig. 6, the peptide induces ERK1/2 kinase activity to enhance endogenous phospho-ERK1/2 levels in NIH 3T3 fibroblasts (*upper panel*) in an MIF-like fashion. Phospho-ERK1/2 levels were analyzed by Western blot with phospho-specific antibody, and ERK1/2 was analyzed for control. Cells were incubated for 0–30 min with the peptides and 0–120 min with full-length MIF (rMIF, latter 3 time points not shown) (*upper panel*), and peptides were tested over a wide concentration range from 0.33 nM to 3.3 μM (*middle panel*). Densitometric analysis of the blots following treatment of the cells with the peptides indicated that phosphorylation of ERK1/2 was stimulated about 2-fold (*top* and

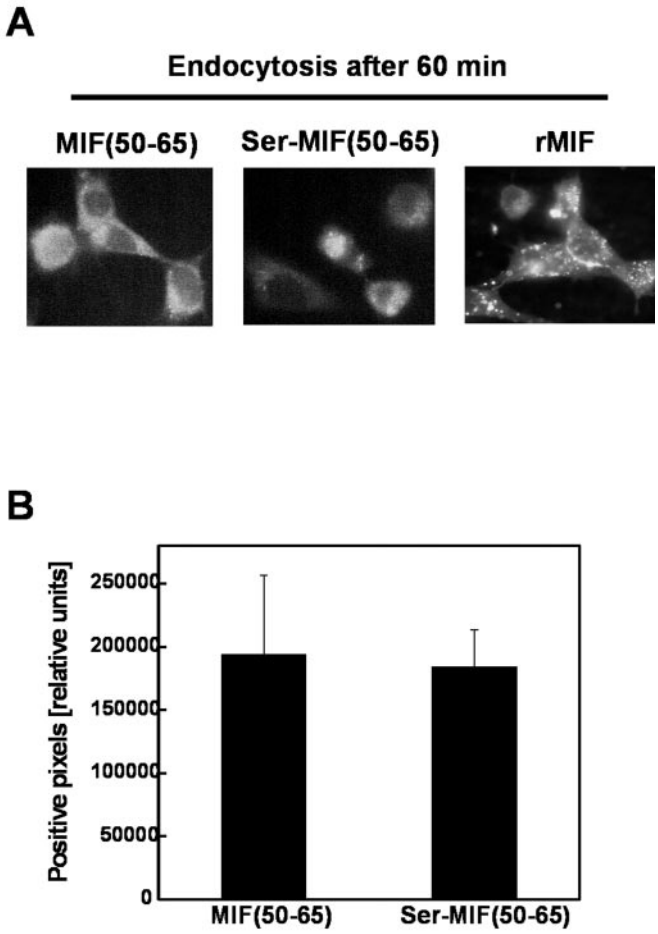

FIG. 8. **MIF-(50–65) and the bis-serine peptide are endocytosed by MIF target cells at comparable rates.** *A*, both fluoresceinated MIF-(50–65) and fluoresceinated C57S/C60S-MIF-(50–65) are endocytosed by NIH 3T3 fibroblasts, but uptake is less efficient than that for fluorescently labeled rMIF. Cell-bound fluorescence after stringent washes was detected to a significant degree within a 60-min cell incubation at 37 °C. Uptake was measured by fluorescence microscopy. The figure shows one representative image out of 9–10 images analyzed per peptide/protein species. *B*, quantification of peptide endocytosis showed that both peptides were endocytosed at a similar efficiency. Quantification was performed by computer-based pixel analysis. The *bars* represent mean values ± S.D. of the pixel analyses from 6 microscopic fields per peptide species.

truncated MIF variants, which retained some of the activities of MIF, consisted of over 100 residues (40, 59).

C-terminal mutants were found to be inactive in the GCOR assay (17, 38). The observation in our current study that MIF-(50–65), which naturally lacks the C terminus of MIF, exhibited GCOR activity indicates that different mechanisms could underlie the GCOR-stimulating activity of MIF and the peptide. On the other hand, previous GCOR studies applying MIF mutants with the C*XX*C cysteines exchanged indicated that the C*XX*C motif or the presence of the cysteines was at least partially necessary for the GCOR activity of MIF. In those studies, no direct proof for an involvement of a redox process was provided, thus leaving it open whether the reduced activity of these mutants was caused by a lack of redox activity or by subtle conformational alterations of the MIF molecule that abolished receptor binding or other MIF-target protein interactions. The observation that the cysteine mutants retained a significant GCOR rest activity of over 30%, also indicated already that additional other stimulatory pathways for MIF-mediated immune cell activation would exist. Together, the previous GCOR studies applying the cysteine and C-terminal mutants of MIF had initially prompted us to hypothesize that C*XX*C-spanning MIF-derived fragments may retain some GCOR activity and possibly other immunological and cellular activities of MIF. Our current study confirms this assumption and demonstrates that the C*XX*C-spanning MIF-derived peptide MIF-(50–65), which consists of only 16 residues, can in fact mimic certain MIF activities.

MIF-(50–65) encompasses residues 50–65 of the MIF sequence. According to the x-ray crystallographic data of human MIF (17), the sequence stretch 50–65 comprises a random coil element followed by a loop, which connects the random coil region with the β4-strand of MIF. In full-length MIF, the random coil region is preceded by the β2- and β3-strands. Our far-UV studies demonstrated that MIF-(50–65) had substantial secondary structure. Reduced MIF-(50–65) was found to be mainly in a random coil conformation. A minimum at 225–227 nm was also present indicating that the reduced form of MIF-(50–65) had a β-turn-forming propensity. Upon oxidation, the portion of β-turn conformation strongly increased as indicated by the absolute increase of the minimum at 225–227 nm. At the same time, the fraction of random coil was markedly diminished. This suggested that disulfide bridge formation induced a β-turn stabilization that was associated with a conformational ordering of the molecule (55). Of note, the side chain-to-side chain lactam-bridged analog of MIF-(50–65) was found to have a strong β-turn conformation. As this analog was designed to form covalent cyclization at the same residues and with the same ring size as for the disulfide-cyclized peptide, it is clear that disulfide-mediated oxidation of the peptide is associated with β-turn stabilization. Conformational ordering might include states consisting of β-strand-β-turn-β-strand or of β-strand-β-turn-α-helix. The latter one is a characteristic motif for the active site of various TPORs. No data on the conformation of the oxidized state of MIF have been available until now. According to the former model, oxidized MIF-(50–65) would contain an antiparallel β-sheet, with the connecting turn conformation and entire structure stabilized by the disulfide bond between Cys^{57} and Cys^{60}. Oxidation-based disulfide formation

middle right panels). C57S/C60S-MIF-(50–65) (Ser-MIF-(50–65)) was almost inactive. Side chain-to-side chain-cyclized MIF-(50–65) (cyclo-MIF-(50–65)) was analyzed in comparison to a linear control peptide to probe for the importance of the β-turn conformation and showed comparable activity as wild-type MIF-(50–65) (*lower panel*). *B*, pull-down analysis demonstrated that MIF-(50–65) directly bound to JAB1. Complexes of biotinylated MIF-(50–65) and *in vitro* translated radiolabeled JAB1 were precipitated with streptavidin-conjugated magnetic beads and bound peptides/proteins analyzed by 13.5% SDS-PAGE and autoradiography as described under "Materials and Methods." An autoradiograph showing radiolabeled JAB1 bands is shown. The biotinylated bis-serine variant of MIF-(50–65) complexed JAB1 to an almost equal degree as MIF-(50–65). Control incubations to account for nonspecific binding were performed without the biotinylated peptides (radiolabeled JAB1 + beads alone = *control*). For control purposes, Western blots of the pull-downs were performed and the biotinylated peptides stained with peroxidase-conjugated streptavidin (pull-down/blotting control; not shown). The autoradiograph shown is representative of 3 independent gels. *C*, both MIF-(50–65) and C57S/C60S-MIF-(50–65) induce $p27^{Kip1}$ stabilization comparable with the effect observed for full-length MIF (rMIF). p27 levels of NIH 3T3 following treatment of cells with rMIF or the peptides were analyzed by 13.5% SDS-PAGE (*left*) and 4–12% NuPAGE (right)/Western blotting with a p27-specific antibody. The effect of MIF-(50–65) was compared with that of the bis-serine variant Ser-MIF-(50–65) over a dose range from 330 nM to 3.3 μM. Control incubations encompassed incubation of cells alone and treatment of cells with the volume of phosphate buffer (NaPP) used in the incubations with the highest peptide concentration. Gel loading was standardized for equal protein concentrations by Bradford analysis. The blots shown are representative of 3–4 independent experiments.

and structural stabilization of MIF-(50–65) was confirmed by the near-UV data, which showed the formation of a maximum between 270 and 285 nm, typical of disulfide bonds. Oxidation-mediated intramolecular disulfide formation in MIF-(50–65) was also verified by mass spectrometric analysis, which showed that the oxidized peptide had a mass that was almost precisely 2 mass units lower than that of the reduced peptide, whereas the obtained fraction of MIF-(50–65) dimers with intermolecular disulfides was neglectable. Stabilization of β-turn formation in oxidized MIF-(50–65) was further confirmed by the CD data obtained for the bis-serine variant of MIF-(50–65). Although NMR studies will ultimately be necessary to obtain detailed information about the conformation stabilized in MIF-(50–65), our CD data obtained for reduced and oxidized MIF-(50–65), the bis-serine mutant, and the side chain-to-side chain lactam-bridged analog together indicate that MIF-(50–65) contains a β-turn-stabilized conformation, likely a β-strand-β-turn-β-strand conformation. Of note, significant β-turn stabilization and conformational ordering via disulfide bridge formation and synthetic constraints has been described previously also for hexa- and octapeptides containing the C*XX*C active sites of the TPORs PDI, Grx, Trx, and Trr (35–37).

We found that MIF-(50–65) had a strong reducing potential with an E'_0 value of −0.258 V. Although the E'_0 value of full-length MIF is unknown, such an electronegative E'_0 value was surprising as it is among the most negative values found for TPORs. For example, the E'_0 value of Trx is −0.270 V and that of Trr is around −0.26 V. It is therefore unlikely that the E'_0 value of MIF is significantly more electronegative than that of the MIF peptide. In fact, we propose that the value of MIF-(50–65) may be taken to get a first approximation of an E'_0 value of MIF. Given that the E'_0 value of MIF might be in the range of approximately −0.25 V, the value for MIF-(50–65) would have been predicted to be more oxidizing, as Moroder and colleagues (35, 36) have shown for most TPORs, that the derived peptide fragments had much more oxidizing redox potentials. For example, linear octapeptides covering the C*XX*C region of Trx and Trr were 60–80 mV more oxidizing than the full-length proteins. This effect was even more pronounced when TPOR-derived hexapeptides were cyclized by covalent N → C bonds. Under such enhanced turn-stabilizing conditions, only the PDI-derived peptide had an E'_0 value that was within the range of that of full-length PDI, whereas the values of the bis-Cys-cyclo peptides derived from Grx, Trx, and Trr were drastically more oxidizing than the full-length proteins (35, 36).

The strong reducing potential observed for MIF-(50–65) implies that the MIF peptide has a strong tendency to become oxidized. The E'_0 potential of MIF-(50–65) as compared with the more oxidizing potentials of other TPOR-derived C*XX*C-containing peptides could be due to the greater length of the MIF-derived peptide. MIF-(50–65) contains 16 residues as compared with the reported 6–8 residues of the peptides of the TPORs. In fact, the CD data indicated a significant turn and, as mentioned, possibly an intramolecular β-sheet-forming propensity, an observation that was in line with the secondary structure prediction according to Garnier (54). Although probably (co-)induced by disulfide formation, the sheet-forming propensity of the peptide could be further assisted by long range interactions in MIF-(50–65), *i.e.* the ends of either β-strand, and could itself in turn facilitate disulfide formation between Cys residues 57 and 60.

In addition, the His residue at position 63 and the neighboring serines could assist disulfide formation by abstracting a proton from Cys^{57} or Cys^{60} or by stabilizing thiolate anion, respectively, with the resulting thiolate anion being able to exert a nucleophilic attack onto the other Cys thiol group. Neighboring His residues have been implicated in influencing the disulfide-forming capacities of C*XX*C cysteines of TPORs (56). On the other hand, neighboring His side chains could favor the formation of mixed disulfides. Whereas MIF-(50–65) forms mixed disulfides with both glutathione and cysteine, the equilibrium fractions of the mixed disulfides are much smaller than for the reported Trx and PDI peptides (35). Among several mechanistic possibilities, this could mean that the His side chain could be involved in both the formation and cleavage of the mixed disulfides.

Only the mixed disulfides of MIF-(50–65) with glutathione occurred in significant amounts at equilibrium. In contrast, the mixed disulfides with cysteine were short living and transient. Compared with peptide fragments of the other TPORs (35), the fraction of mixed disulfides formed by MIF-(50–65) was small. This finding is consistent with the measured negative E'_0 value of MIF-(50–65).

S-Thiolation of MIF-(50–65) could be indicative of a potential *S*-thiolation of full-length MIF in the cell, which in turn may have functional relevance in cellular redox regulation. Interestingly, glycosylation-inhibiting factor (GIF), a mediator homologous to MIF, has been shown to be cysteinylated at Cys^{60}, and cysteinylation of GIF has been suggested to represent a functional post-translational modification of GIF (63). Trx was recently demonstrated to become glutathionylated under conditions of oxidative stress. Glutathionylation was detected to occur at Cys^{72} of Trx but not at the C*XX*C cysteine residues (64). Given this latter observation made for Trx, it is therefore unclear whether glutathionylation of MIF-(50–65), which occurred at Cys^{57}, Cys^{60}, or both C*XX*C Cys residues, could be an indication for glutathionylation of MIF in the cell. Nevertheless, the data obtained in our study in conjunction with the reports on the cysteinylation and glutathionylation of GIF and Trx, respectively, warrant further studies addressing the issue of a potential *S*-thiolation of cellular MIF. MIF-mediated class II antigen processing (21) could also involve *S*-thiolation of MIF as a transition state.

The strongly negative redox potential of MIF-(50–65) suggests that the redox activity could be critical for the biological activities observed for the peptide. Although this is possible and, given our knowledge on the connection between the redox activity of full-length MIF and its immunological effects (19, 22, 23), even likely, the current study gives no final proof for this notion, because the applied bis-serine variant was not found to be inactive in all biological assays performed. For example, C57S/C60S-MIF-(50–65) bound to JAB1 similar to MIF-(50–65) and exhibited p27-stabilizing properties comparable with the wild-type peptide. Moreover, the observation that cysteine-less cyclo-MIF was able to activate ERK phosphorylation indicated that for at least some MIF target proteins, disulfide formation could rather have conformational functions (see proposed molecular model below).

The native-like biological activity of MIF-(50–65) was demonstrated using a number of relevant biological assays. Glucocorticoid overriding has been shown to be a unique property of MIF and represents an important mechanistic principle through which MIF can exert its specific pro-inflammatory spectrum of activities (3). The observation made in this study that the MIF peptide exhibited GCOR activity is therefore probably the most important finding to indicate that MIF-(50–65) can exert native-like MIF activities. Enhancement by MIF of cell proliferation has also been widely demonstrated, and this activity of MIF has been suggested to be associated with a role of MIF as a tumor growth promoter (5). We applied a cell proliferation assay based on the use of primary cells. MIF-(50–

65), like MIF, led to an increase in proliferation of bFGF- and VEGF-stimulated MVECs. Because primary cells were used for this assay and because MIF has been implicated in endothelial cell regulation and atherogenesis (15), this result further demonstrated the relevance of the activity profile found for the peptide.

MAPK activation by MIF and modulation of JAB1 pathways have been among the very few molecular machineries identified for MIF signaling to date. We used assays addressing either activity branch in our study. Quite surprisingly, MIF-(50–65) not only led to phosphorylation of ERK1/2 but also was found to stimulate this activity within a few minutes. This indicated that the peptide could have acted as an agonist for the putative MIF receptor.

It has been demonstrated that MIF can be taken up by target cells through an apparently receptor-independent endocytosis pathway. As mentioned, the fast mode of action on ERK1/2 activation which MIF-(50–65) shares with MIF argues, however, that the peptide directly acts on a cell surface protein to trigger a typical, fast signaling event. By contrast, peptide activity on p27 stabilization could occur via a different, independent pathway, as these experiments were performed for several hours. Endocytosis studies showed that both MIF-(50–65) and the bis-serine variant are taken up by typical MIF target cells and that uptake was less efficient than that for full-length MIF. Significant and comparable endocytosis could be measured for both peptides and occurred within 60 min, suggesting that the different structure activity profiles of MIF-(50–65) and its serine variant are not due to different endocytosis rates. It is currently unclear how endocytosis of the peptides and signaling are connected. Also it is not yet clear why uptake of MIF is more efficient. As the difference in the fluorescence labeling ratio can probably not fully account for the different uptake rates between MIF and the peptides, we conclude that mechanistic differences may exist. The concentration and kinetic profiles of the MIF and peptide activities in the various assays applied do not yet allow for a unifying mechanistic picture in discerning receptor-mediated *versus* intracellular signaling-mediated and C*XX*C-based *versus* sequence-based effects. Detailed kinetic studies on MIF and the peptides in comparison to cyclo-MIF-(50–65) and other analogs will have to be performed in the future to further clarify this point.

The most active concentrations of MIF-(50–65) were different over the assays performed. Optimal GCOR and MVEC growth-stimulatory activity was obtained with ~3 μM peptide. In contrast, a tenth of this concentration (330 nM) resulted in maximal induction of ERK1/2 phosphorylation. The peptide concentrations necessary for the biological effect to be observed were lower than those of full-length MIF throughout, but although the potency of the peptide was ~1000-fold lower in the GCOR assay, the activities of MIF and the peptide were within the same range in the MAPK activation and the p27 stabilization assays (~4–40- and 3-fold difference, respectively). The observed differences between the assays could well represent the different molecular pathways addressed, as also the optimal concentrations of MIF varied. For example, micromolar concentrations of MIF have been suggested previously (5, 6) to be associated with the enzymatic effects of MIF. Also, different endocytosis efficiencies could underlie these differences, as rMIF was observed to be endocytosed at a much stronger rate.

Given its *in vitro* catalytic activity and its MIF-like immunological and cellular activities, as demonstrated in this study, MIF-(50–65) represents a dramatically minimized MIF analog of only 16 amino acids compared with the 114 residues of full-length MIF. Although this minimization is dramatic and surprising, protein minimization efforts have recently led to the identification of a number of small peptides, domains, and motifs that are able to cover a significant spectrum of the activities of the parent proteins. As discussed above, a number of TPOR-derived peptides of a little as 6 residues have been described. However, so far these peptides have only been shown to share the catalytic oxidoreductase and refolding activity with the full-length TPORs (35, 36). A 12-amino acid-long synthetic peptide, designed and selected as an Mdm2-binding protein, was shown to bind to the p53 binding pocket on the Mdm2 protein. The mini Mdm2-binding protein, which apparently effectively competes with the native protein, stabilized p53 and led to an activation of the p53 response (65).

Although some of the biological activities measured for MIF-(50–65) were obtained by peptide concentrations that were within the range of those used for rMIF, *i.e.* 3 μM of peptide had about the same MVEC-stimulatory effect as 400 nM rMIF, overall the peptide seemed to have a lower potency than full-length MIF in most assays performed in this study. However, this was not surprising as small peptide sequences, due to their lack of three-dimensional structure, often show reduced affinities and activities compared with their parent molecules. For example, a minimized transforming growth factor-α peptide, truncated by 8 out of 50 residues, had a 10-fold lower affinity for the receptor than the native molecule (66). A mini-proinsulin molecule consisting of one chain shows native foldability but only had a 1500-fold lower receptor binding affinity and had no biological activity (67).

There are at least two examples in the literature demonstrating striking protein minimization with the resulting minimized molecules exhibiting potent native-like activities, although their sequence/structure is not found in the sequence of the native molecules. A 14-residue peptide was selected by phage display as a potent agonist of erythropoietin that could stimulate erythropoiesis. The signaling pathways activated by this erythropoietin agonistic peptide appeared to be identical to those induced by the native hormone (68). Arkin *et al.* (69) recently identified a non-peptidyl small molecule, which bound to the cytokine interleukin-2 through mimicking the protein-protein interface that the interleukin-2 receptor-α-subunit shares with interleukin-2. The small molecule was able to behave adaptively in binding to the predicted dynamic protein interface. This work as well as studies on the characterization of ligand-receptor interfaces such as those of the growth hormone-growth hormone receptor extracellular domain (70) have demonstrated that ligand receptor interfaces sufficient for receptor activation can be as small as to only cover a few amino acid residues. Thus, the 16-residue-comprising MIF peptide may well provide sufficient "conformational properties" to make up for a receptor-binding epitope or to represent a docking site for a redox protein target of MIF or to represent the MIF-docking site for JAB1 binding (14). Discrete folding of mini-proteins or mini-domains has been demonstrated for a number of proteins (71), further confirming that MIF-(50–65) could be discretely folded to exert native-like activities on target proteins.

Nevertheless, the current study leaves it open through which molecular mechanism MIF-(50–65) exhibits its MIF-like biological activities. In fact, the 16-meric peptide could act via different pathways. It could bind to a cell surface receptor and modulate receptor activity through this binding event. In favor of such a mechanistic concept are structural analyses of MIF, indicating that the region around residue Cys^{60} is surface-exposed (17). On the other hand, our current study in conjunction with previous data (14) indicates that, in addition, the peptide could bind to JAB1, resulting in the modulation of JAB1-mediated MIF-regulatory pathways. Another intriguing

mechanistic possibility is suggested by a recent report (21) showing that MIF interacts with MHC II molecules and can act to process class-restricted peptides in a disulfide-mediated manner. Accordingly, MIF and thus the MIF-derived C*XX*C-spanning peptide could act through the MHC II machinery.

The observed conversion of reduced MIF-(50–65), from a mostly unordered molecule containing a predominant fraction of random coil structure into an oxidized species with marked β-turn structure, indicated that the MIF peptide could potentially dock onto target proteins such as insulin, JAB1, or the putative receptor. Such a binding event could initially involve a mainly unordered conformation, and upon binding or oxidation, the peptide could become ordered. As mentioned, such a mechanism has been proposed to be part of the redox mechanism of Trr (39), a TPOR enzyme that does not contain a helix-loop-strand Trx-fold. Our initial bioactivity data obtained for the side chain-to-side chain cyclized MIF peptide analog would be in favor of such a molecular model. Cyclo-MIF-(50–65) contains a synthetic constraint to stabilize a β-turn conformational element but does not have any cysteine residues, which could be involved in redox reactions. Yet cyclo-MIF-(50–65) showed an ERK-stimulatory activity that was comparable with that of MIF-(50–65). The bis-serine variant of the peptide as well as several C*XX*C mutants of full-length MIF show impaired immunological activity, but the bis-serine peptide binds JAB1 and enhances p27 levels. At first sight, these observations do not appear to fit within one mechanistic model. However, the following model may apply; MIF approaches target proteins such as the putative membrane receptor in its reduced state. Reduced MIF may be maintained by several conditions in both the intra- and extracellular milieu including autocrine loops, local reduced-state environments around macrophages, or the reducing capacity of the cytosol. Binding to a membrane receptor would then require reduction of the receptor or an adjacent co-receptor disulfide structure with the concomitant oxidation of the MIF C*XX*C cysteines. Through this mechanism disulfide oxidation of MIF would be associated with β-turn and loop formation, which would then be necessary but also sufficient for receptor binding *per se*. The latter scenario would be fully compatible with our finding that cyclo-MIF-(50–65) triggers ERK activation. At the same time, (co-)receptor reduction by MIF could participate in a conformational modulation needed for signal transduction. Our data also imply that MIF modulation of the JAB1 target protein probably involves another or a simpler molecular process.

The clarification of these issues will have to await the precise elucidation of the signaling pathways of full-length MIF. Although the recent identification of an involvement of the MAPK, JAB1, and p53 pathways (13, 14, 72) has been revealing, it is likely that the majority of cellular pathways and interaction partners of MIF signaling has remained elusive.

Irrespective of these challenges to be addressed in future studies, we draw two conclusions from this work. First, MIF-(50–65) could represent a valuable experimental tool for future investigations as to the elucidation of the molecular pathways of MIF action. For example, the peptide could be used for receptor cross-linking studies. Given the conformational susceptibility of full-length MIF to experimental treatment (22), the peptide would be much more readily amenable to modifications and experimental handling as compared with the full-length protein. Second, MIF-(50–65) could serve as a useful molecular template for the design of peptidyl or non-peptidyl small molecule drugs with MIF-regulating functions. Such compounds could be extremely useful therapeutically, as MIF has been shown to be a critical mediator of several immune and inflammatory diseases.

Acknowledgments—We thank F. Vitzthum for help with the design of the redox equilibrium experiments; M. Krampert for recording CD spectra; M. Bergmann and T. Kazantzis for help with the peptide synthesis; and A. Burger-Kentischer, G. Geiger, and D. Finkelmeier for help with the pull-down experiments. We are grateful to R. W. Frank, J. Schmucker, K. Borchers, G. Tovar, and W. Voelter for assistance with the mass spectrometric measurements; M. Thiele and A. Schober for help with the endocytosis analysis; and M. Dewor for performing the amino acid analyses.

REFERENCES

1. David, J. R. (1966) *Proc. Natl. Acad. Sci. U. S. A.* **56,** 72–77
2. Bernhagen, J., Calandra, T., Mitchell, R. A., Martin, S. B., Tracey, K. J., Voelter, W., Manogue, K. R., Cerami, A., and Bucala, R. (1993) *Nature* **365,** 756–759
3. Calandra, T., Bernhagen, J., Metz, C. N., Spiegel, L. A., Bacher, M., Donnelly, T., Cerami, A., and Bucala, R. (1995) *Nature* **377,** 68–71
4. Bucala, R. (1996) *FASEB J.* **10,** 1607–1613
5. Mitchell, R. A., and Bucala, R. (2000) *Semin. Cancer Biol.* **10,** 359–366
6. Lue, H., Kleemann, R., Calandra, T., Roger, T., and Bernhagen, J. (2002) *Microb. Infect.* **4,** 449–460
7. Bozza, M., Satoskar, A. R., Lin, G., Lu, B., Humbles, A. A., Gerard, C., and David, J. R. (1999) *J. Exp. Med.* **189,** 341–346
8. Calandra, T., Echtenacher, B., Le Roy, D., Pugin, J., Metz, C. N., Hültner, L., Heumann, D., Männel, D., Bucala, R., and Glauser, M. (2000) *Nat. Med.* **6,** 164–169
9. Mikulowska, A., Metz, C. N., Bucala, R., and Holmdahl, R. (1997) *J. Immunol.* **158,** 5514–5517
10. Takahashi, N., Nishihira, J., Sato, Y., Kondo, M., Ogawa, H., Ohshima, T., Une, Y., and Todo, S. (1998) *Mol. Med.* **4,** 707–714
11. Chesney, J., Metz, C., Bacher, M., Peng, T., Meinhardt, A., and Bucala, R. (1999) *Mol. Med.* **5,** 181–191
12. Donnelly, S. C., Haslett, C., Reid, P. T., Grant, I. S., Wallace, W. A., Metz, C. N., Bruce, L. J., and Bucala, R. (1997) *Nat. Med.* **3,** 320–323
13. Mitchell, R. A., Metz, C. N., Peng, T., and Bucala, R. (1999) *J. Biol. Chem.* **274,** 18100–18106
14. Kleemann, R., Hausser, A., Geiger, G., Mischke, R., Burger-Kentischer, A., Flieger, O., Johannes, F. J., Roger, T., Calandra, T., Kapurniotu, A., Grell, M., Finkelmeier, D., Brunner, H., and Bernhagen, J. (2000) *Nature* **408,** 211–216
15. Burger-Kentischer, A., Goebel, H., Seiler, R., Fraedrich, G., Schaefer, H. E., Dimmeler, S., Kleemann, R., Bernhagen, J., and Ihling, C. (2002) *Circulation* **105,** 1561–1566
16. Ellis, L. B. M., Saurugger, P., and Woodward, C. (1992) *Biochemistry* **31,** 4882–4891
17. Sun, H., Bernhagen, J., Bucala, R., and Lolis, E. (1996) *Proc. Natl. Acad. Sci. U. S. A.* **93,** 5191–5196
18. Sugimoto, H., Suzuki, M., Nakagawa, A., Tanaka, I., and Nishihira, J. (1996) *FEBS Lett.* **389,** 145–148
19. Kleemann, R., Kapurniotu, A., Frank, R. W., Gessner, A., Mischke, R., Flieger, O., Jüttner, S., Brunner, H., and Bernhagen, J. (1998) *J. Mol. Biol.* **280,** 85–102
20. Kleemann, R., Mischke, R., Kapurniotu, A., Brunner, H., and Bernhagen, J. (1998) *FEBS Lett.* **430,** 191–196
21. Potolicchio, I., Santambrogio, L., and Strominger, J. L. (2003) *J. Biol. Chem.* **278,** 30889–30895
22. Kleemann, R., Kapurniotu, A., Mischke, R., Held, J., and Bernhagen, J. (1999) *Eur. J. Biochem.* **261,** 753–766
23. Kleemann, R., Rorsman, H., Rosengren, E., Mischke, R., Mai, N. T., and Bernhagen, J. (2000) *Eur. J. Biochem.* **267,** 7183–7193
24. Jung, H., Kim, T., Chae, H. Z., Kim, K. T., and Ha, H. (2001) *J. Biol. Chem.* **276,** 15504–15510
25. Nguyen, M., Lue, H., Kleemann, R., Thiele, M., Tolle, G., Finkelmeier, D., Wagner, E., Braun, A., and Bernhagen, J. (2003) *J. Immunol.* **170,** 3337–3347
26. Bucala, R. (2000) *Nature* **408,** 167–168
27. Tagaya, Y., Maeda, Y., Mitsui, A., Kondo, Matsui, H., Hamuro, J., Brown, R., Arai, K., Yokota, T., Wakasugi, N., and Yodoi, J. (1989) *EMBO J.* **8,** 757–764
28. Tanaka, T., Nakamura, H., Nishiyama, A., Hosoi, F., Masutani, H., Wada, H., and Yodoi, J. (2000) *Free Radic. Res.* **33,** 851–855
29. Bertini, R., Howard, O. M. Z., Dong, H.-F., Oppenheim, J. J., Bizzarri, C., Caselli, G., Pagliei, S., Romines, B., Wilshire, J. A., Mengozzi, M., Nakamura, H., Yodoi, J., Pekkari, K., Gurunath, R., Holmgren, A., Herzenberg, L. A., Herzenberg, L. A., and Ghezzi, P. (1999) *J. Exp. Med.* **189,** 1783–1789
30. Pekkari, K., Gurunath, R., Arner, E. S., and Holmgren, A. (2000) *J. Biol. Chem.* **275,** 37474–37480
31. Krause, G., Lundström, J., Barea, J. L., Pueyo de la Cuesta, C., and Holmgren, A. (1991) *J. Biol. Chem.* **266,** 9494–9500
32. Chivers, P. T., Laboissiere, M. C. A., and Raines, R. T. (1996) *EMBO J.* **15,** 2659–2667
33. Huber-Wunderlich, M., and Glockshuber, R. (1998) *Folding Des.* **3,** 161–171
34. Zhang, R., and Snyder, G. H. (1989) *J. Biol. Chem.* **264,** 18472–18479
35. Cabrele, C., Flori, S., Pegoraro, S., and Moroder, L. (2002) *Chem. Biol.* **9,** 731–740
36. Siedler, F., Rudolph-Böhner, S., Doi, M., Musiol, H. J., and Moroder, L. (1993) *Biochemistry* **32,** 7488–7495
37. Siedler, F., Quarzago, D., Rudolph-Bohner, S., and Moroder, L. (1994) *Biopolymers* **34,** 1563–1572
38. Mischke, R., Kleemann, R., Brunner, H., and Bernhagen, J. (1998) *FEBS Lett.* **427,** 85–90

39. Waksman, G., Krishna, T. S., Williams, C. H. J., and Kuriyan, J. (1994) *J. Mol. Biol.* **236,** 800–816
40. Mischke, R., Gessner, A., Kapurniotu, A., Jüttner, S., Kleemann, R., Brunner, H., and Bernhagen, J. (1997) *FEBS Lett.* **414,** 226–232
41. Maciag, T., Cerundolo, J., Ilsley, S., Kelley, P. R., and Forand, R. (1979) *Proc. Natl. Acad. Sci. U. S. A.* **76,** 5674–5678
42. Kazantzis, A., Waldner, M., Taylor, J. W., and Kapurniotu, A. (2002) *Eur. J. Biochem.* **269,** 780–791
43. Soulimane, T., Than, M. E., Dewor, M., Huber, R., and Buse, G. (2000) *Protein Sci.* **9,** 2068–2073
44. Weston, R. E., and Schwarz, H. A. (1972) *Chemical Kinetics*, Prentice-Hall, Englewood Cliffs, NJ
45. Szajewski, R. P., and Whitesides, G. M. (1980) *J. Am. Chem. Soc.* **102,** 2011–2026
46. Millis, K. K., Weaver, K. H., and Rabenstein, D. L. (1993) *J. Org. Chem.* **58,** 4144–4146
47. Holmgren, A. (1979) *J. Biol. Chem.* **254,** 9627–9632
48. Rosengren, E., Bucala, R., Åman, P., Jacobsson, L., Odh, G., Metz, C. N., and Rorsman, H. (1996) *Mol. Med.* **2,** 143–149
49. Defillippi, P., van Hinsbergh, V. W. M., Bertolotto, A., Rossino, P., Silengo, L., and Tarone, G. (1991) *J. Cell Biol.* **114,** 855–863
50. Draijer, R., Atsma, D. E., van der Laarse, A., and van Hinsbergh, V. W. (1995) *Circ. Res.* **76,** 199–208
51. van Hinsbergh, V. W., Vermeer, M., Koolwijk, P., Grimbergen, J., and Kooistra, T. (1994) *Blood* **84,** 2984–2991
52. Bradford, M. (1976) *Anal. Biochem.* **72,** 248–256
53. Smith, J. A., and Pease, L. G. (1980) *CRC Crit. Rev. Biochem.* **8,** 315–399
54. Garnier, J., Osguthorpe, D. J., and Robson, B. (1978) *J. Mol. Biol.* **120,** 97–120
55. Rose, D. G., Gierasch, L. M., and Smith, J. A. (1985) *Adv. Protein Chem.* **37,** 1–109
56. Bulaj, G., Kortemme, T., and Goldenberg, D. P. (1998) *Biochemistry* **37,** 8965–8972
57. Fomenko, D. E., and Gladyshev, V. N. (2002) *Protein Sci.* **11,** 2285–2296
58. Woody, R. W. (1985) *Peptides* (*Orlando*) **7,** 15–113
59. Bendrat, K., Alabed, Y., Callaway, D. J. E., Peng, T., Calandra, T., Metz, C. N., and Bucala, R. (1997) *Biochemistry* **36,** 15356–15362
60. Fingerle-Rowson, G., Koch, P., Bikoff, R., Lin, X., Metz, C. N., Dhabhar, F. S., Meinhardt, A., and Bucala, R. (2003) *Am. J. Pathol.* **162,** 47–56
61. Swope, M., Sun, H.-W., Blake, P. R., and Lolis, E. (1998) *EMBO J.* **1,** 3534–3541
62. Lubetsky, J. B., Swope, M., Dealwis, C., Blake, P., and Lolis, E. (1999) *Biochemistry* **38,** 7346–7354
63. Watarai, H., Nozawa, R., Tokunaga, A., Yuyama, N., Tomas, M., Hinohara, A., Ishizaka, K., and Ishii, Y. (2000) *Proc. Natl. Acad. Sci. U. S. A.* **97,** 13251–13256
64. Casagrande, S., Bonetto, V., Fratelli, M., Gianazza, E., Eberini, I., Massignan, T., Salmona, M., Chang, G., Holmgren, A., and Ghezzi, P. (2002) *Proc. Natl. Acad. Sci. U. S. A.* **99,** 9745–9749
65. Bottger, A., Bottger, V., Sparks, A., Liu, W. L., Howard, S. F., and Lane, D. P. (1997) *Curr. Biol.* **7,** 860–869
66. McInnes, C., Wang, J., Al Moustafa, A. E., Yansouni, C., O'Connor-McCourt, M., and Sykes, B. D. (1998) *J. Biol. Chem.* **273,** 27357–27363
67. Hua, Q. X., Hu, S. Q., Jia, W., Chu, Y. C., Burke, G. T., Wang, S. H., Wang, R. Y., Katsoyannis, P. G., and Weiss, M. A. (1998) *J. Mol. Biol.* **277,** 103–118
68. Wrighton, N. C., Farrell, F. X., Chang, R., Kashyap, A. K., Barbone, F. P., Mulcahy, L. S., Johnson, D. L., Barrett, R. W., Jolliffe, L. K., and Dower, W. J. (1996) *Science* **273,** 458–463
69. Arkin, M. R., Randal, M., DeLano, W. L., Hyde, J., Luong, T. N., Oslob, J. D., Raphael, D. R., Taylor, L., Wang, J., McDowell, R. S., Wells, J. A., and Braisted, A. C. (2003) *Proc. Natl. Acad. Sci. U. S. A.* **100,** 1603–1608
70. de Vos, A. M., Ultsch, M., and Kossiakoff, A. A. (1992) *Science* **255,** 306–312
71. Martin, L., and Vita, C. (2000) *Curr. Protein Pept. Sci.* **1,** 403–430
72. Hudson, J. D., Shoaibi, M. A., Maestro, R., Carnero, A., Hannon, G. J., and Beach, D. H. (1999) *J. Exp. Med.* **190,** 1375–1382

A 16-Residue Peptide Fragment of Macrophage Migration Inhibitory Factor, MIF-(50–65), Exhibits Redox Activity and Has MIF-like Biological Functions

Mai Tuyet Nguyen, Jürgen Beck, Hongqi Lue, Helge Fünfzig, Robert Kleemann, Pieter Koolwijk, Aphrodite Kapurniotu and Jürgen Bernhagen

J. Biol. Chem. 2003, 278:33654-33671.
doi: 10.1074/jbc.M301735200 originally published online June 9, 2003
